

**Journal of Computational Neuroscience**

**A BIOPHYSICAL MODEL OF THE CORTEX-BASAL GANGLIA-THALAMUS NETWORK IN THE 6-OHDA LESIONED RAT MODEL OF PARKINSON'S DISEASE**

--Manuscript Draft--

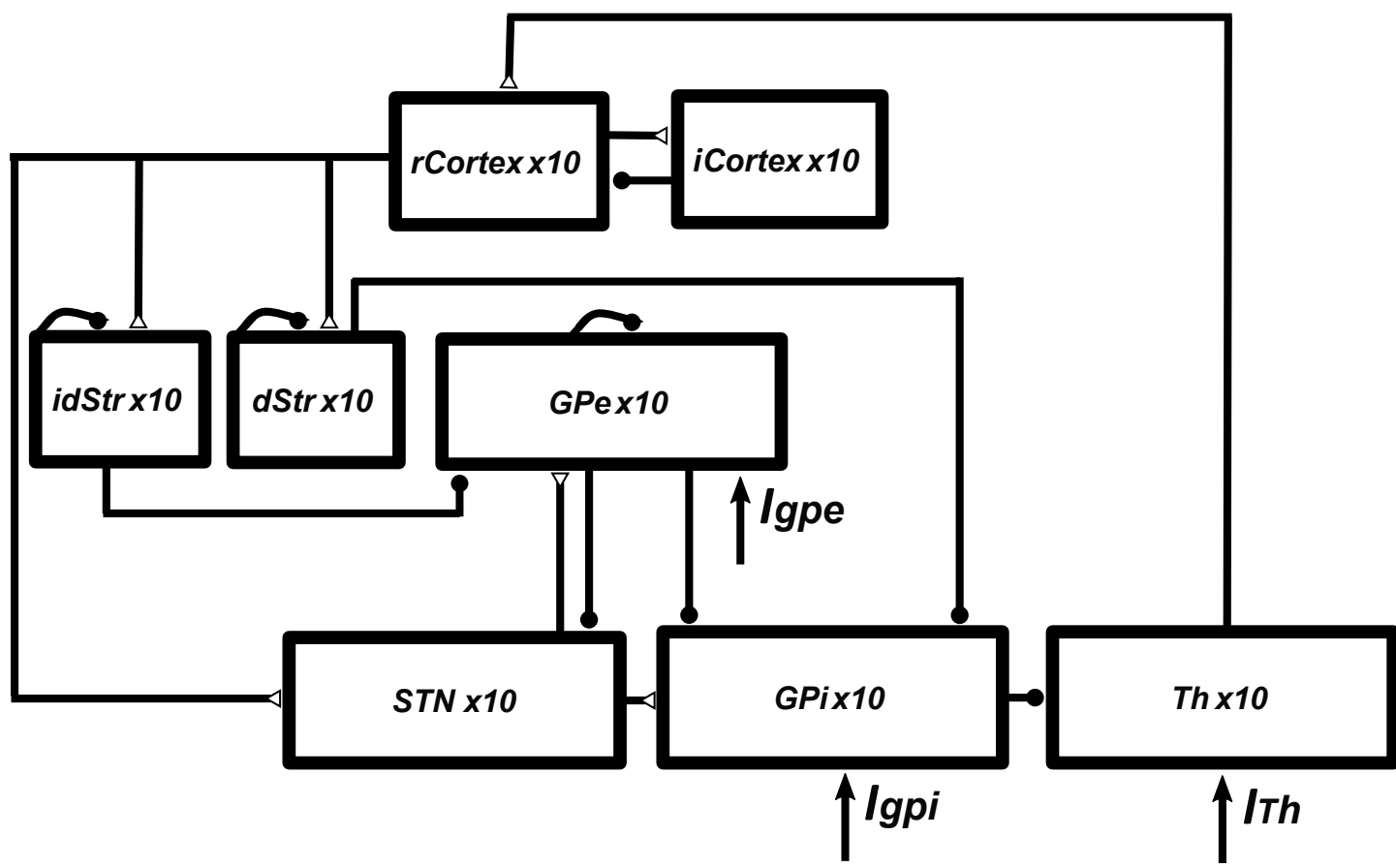
<b>Manuscript Number:</b>	JCNS-D-15-00110	
<b>Full Title:</b>	A BIOPHYSICAL MODEL OF THE CORTEX-BASAL GANGLIA-THALAMUS NETWORK IN THE 6-OHDA LESIONED RAT MODEL OF PARKINSON'S DISEASE	
<b>Article Type:</b>	Original Article	
<b>Keywords:</b>	Deep brain stimulation - Parkinson's disease - 6-OHDA lesioned rat model - Subthalamic nucleus - Computational model - Pathological oscillatory activity	
<b>Corresponding Author:</b>	Warren M. Grill, Ph.D. Duke University Durham, NC UNITED STATES	
<b>Corresponding Author Secondary Information:</b>		
<b>Corresponding Author's Institution:</b>	Duke University	
<b>Corresponding Author's Secondary Institution:</b>		
<b>First Author:</b>	Karthik Kumaravelu	
<b>First Author Secondary Information:</b>		
<b>Order of Authors:</b>	Karthik Kumaravelu  David Brocker  Warren Grill	
<b>Order of Authors Secondary Information:</b>		
<b>Funding Information:</b>	National Institute of Neurological Disorders and Stroke (NIH R37 NS040894)	Warren Grill
	National Institute of Neurological Disorders and Stroke (NIH R01 NS079312)	Warren Grill
<b>Abstract:</b>	<p>Electrical stimulation of sub-cortical brain regions (the basal ganglia), known as deep brain stimulation (DBS), is an effective treatment for Parkinson's disease (PD). Chronic high frequency (HF) DBS in the subthalamic nucleus (STN) or globus pallidus interna (GPI) reduces motor symptoms including bradykinesia and tremor in patients with PD, but the therapeutic mechanisms of DBS are not fully understood. We developed a biophysical network model comprising of the closed loop cortical-basal ganglia-thalamus circuit representing the healthy and parkinsonian rat brain. The network properties of the model were validated by comparing responses evoked in basal ganglia (BG) nuclei by cortical (CTX) stimulation to published experimental results. A key emergent property of the model was generation of low-frequency network oscillations. Consistent with their putative pathological role, low-frequency oscillations in model BG neurons were exaggerated in the parkinsonian state compared to the healthy condition. We used the model to quantify the effectiveness of STN DBS at different frequencies in suppressing low-frequency oscillatory activity in GPI. Frequencies less than 40 Hz were ineffective, low-frequency oscillatory power decreased gradually for frequencies between 50 Hz and 130 Hz, and saturated at frequencies higher than 150 Hz. HF STN DBS suppressed pathological oscillations in GPe/GPi both by exciting and inhibiting the firing in GPe/GPi neurons, and the number of GPe/GPi neurons influenced was greater for HF stimulation than low-frequency stimulation. Similar to the frequency dependent suppression of pathological oscillations, STN DBS also normalized the abnormal GPI spiking activity evoked by CTX stimulation in a frequency dependent fashion with HF being the most effective. Therefore, therapeutic HF STN DBS effectively suppresses pathological activity by</p>	

	<p>influencing the activity of a greater proportion of neurons in the output nucleus of the BG.</p>
<b>Suggested Reviewers:</b>	<p>Christopher Butson butson@sci.utah.edu Research area is computational modeling of Deep Brain Stimulation to treat Parkinson's disease.</p> <p>Matthew Johnson john5101@umn.edu Research area is computational modeling of Deep Brain Stimulation to treat Parkinson's disease.</p> <p>Madeleine Lowery madeleine.lowery@ucd.ie Research area is computational modeling of Deep Brain Stimulation to treat Parkinson's disease.</p> <p>Eric Shea Brown etsb@washington.edu Research area is computational modeling of Deep Brain Stimulation to treat Parkinson's disease.</p> <p>Michelle McCarthy mmccart@math.bu.edu Research area is computational modeling of Deep Brain Stimulation to treat Parkinson's disease.</p>
<b>Opposed Reviewers:</b>	<p>Erwin B Montgomery  Long-standing scientific dispute.</p>

● Glutamate

● GABA

→ Bias Current



B

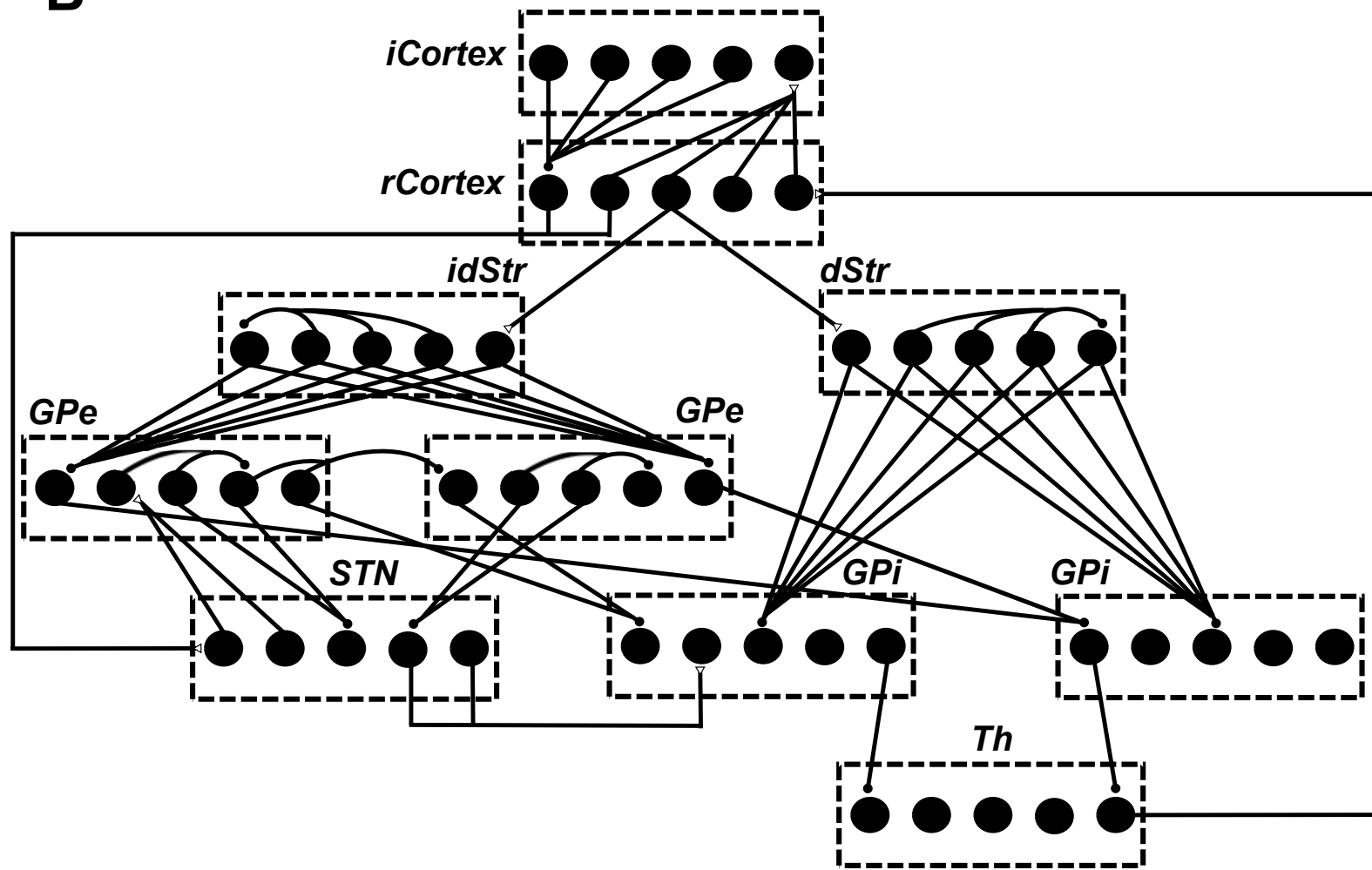
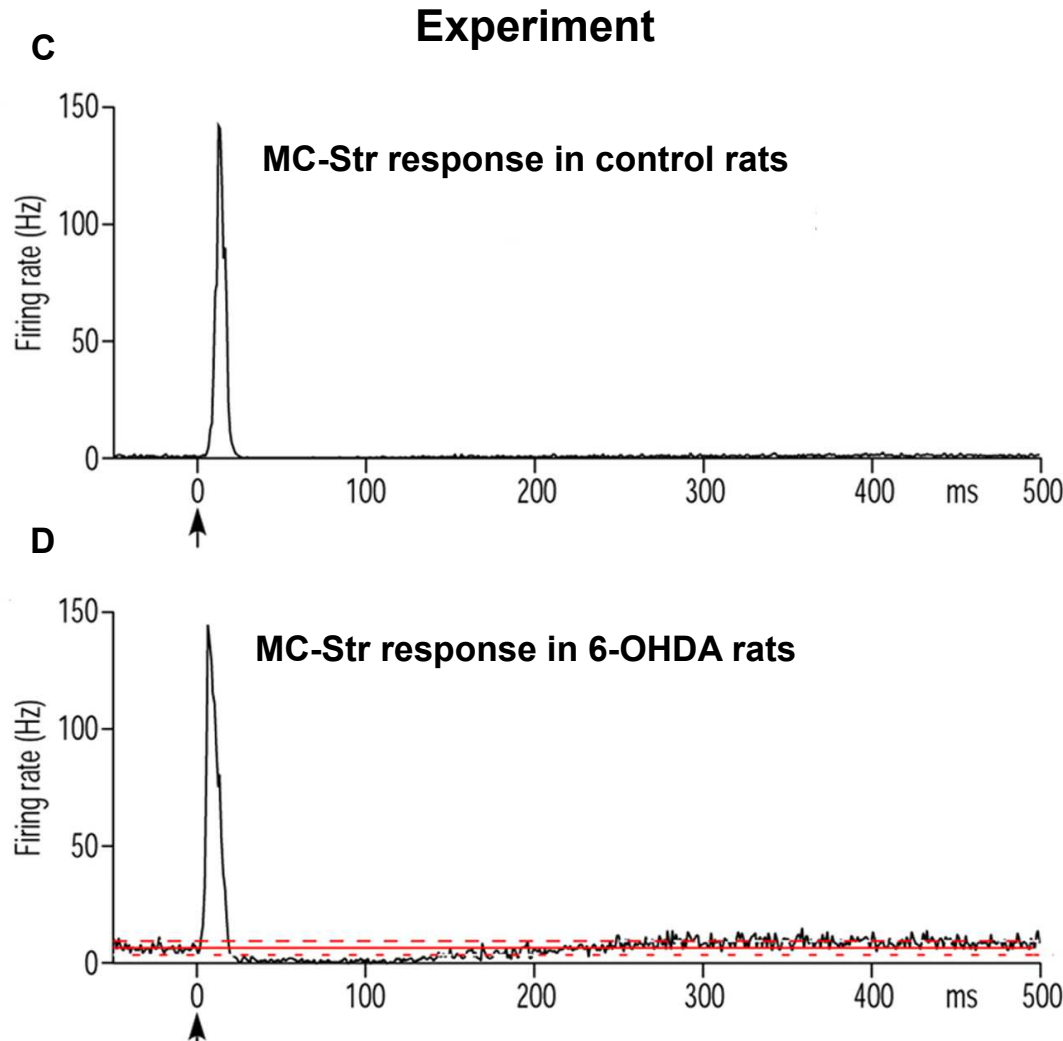
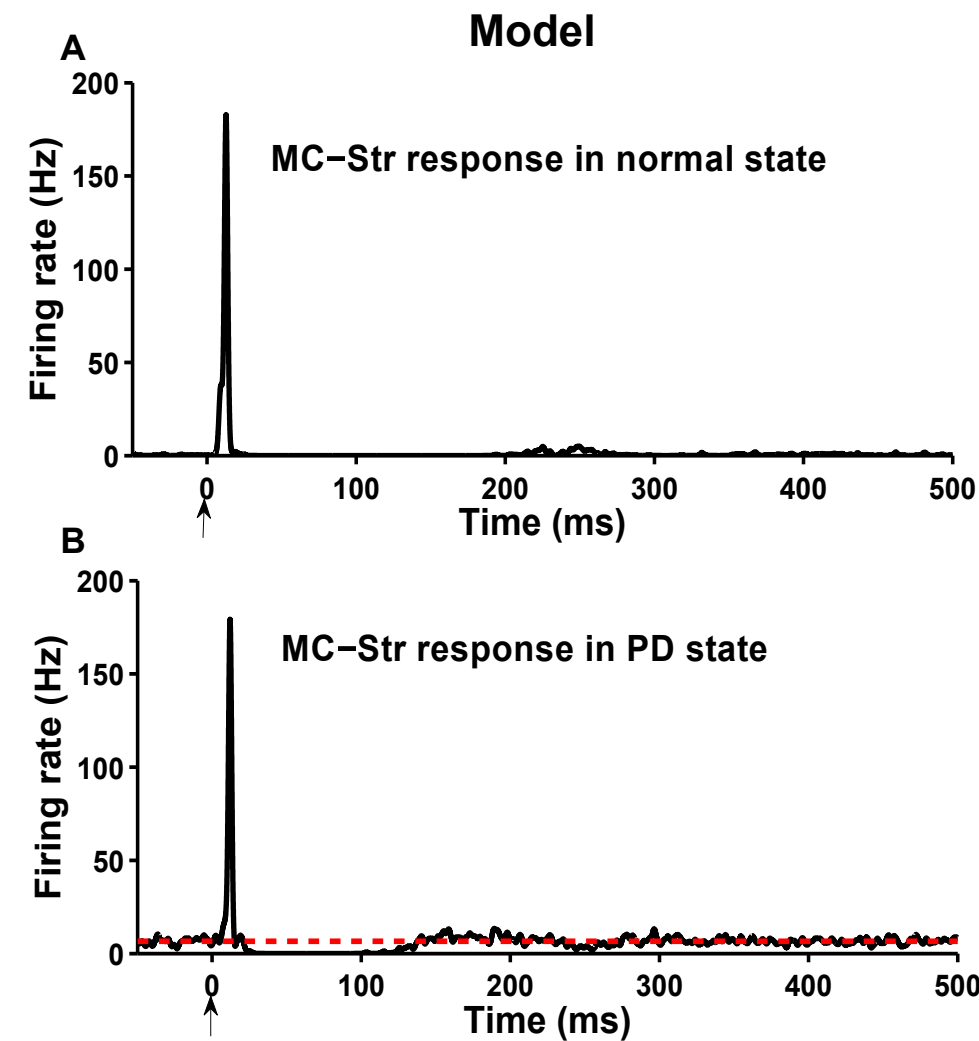
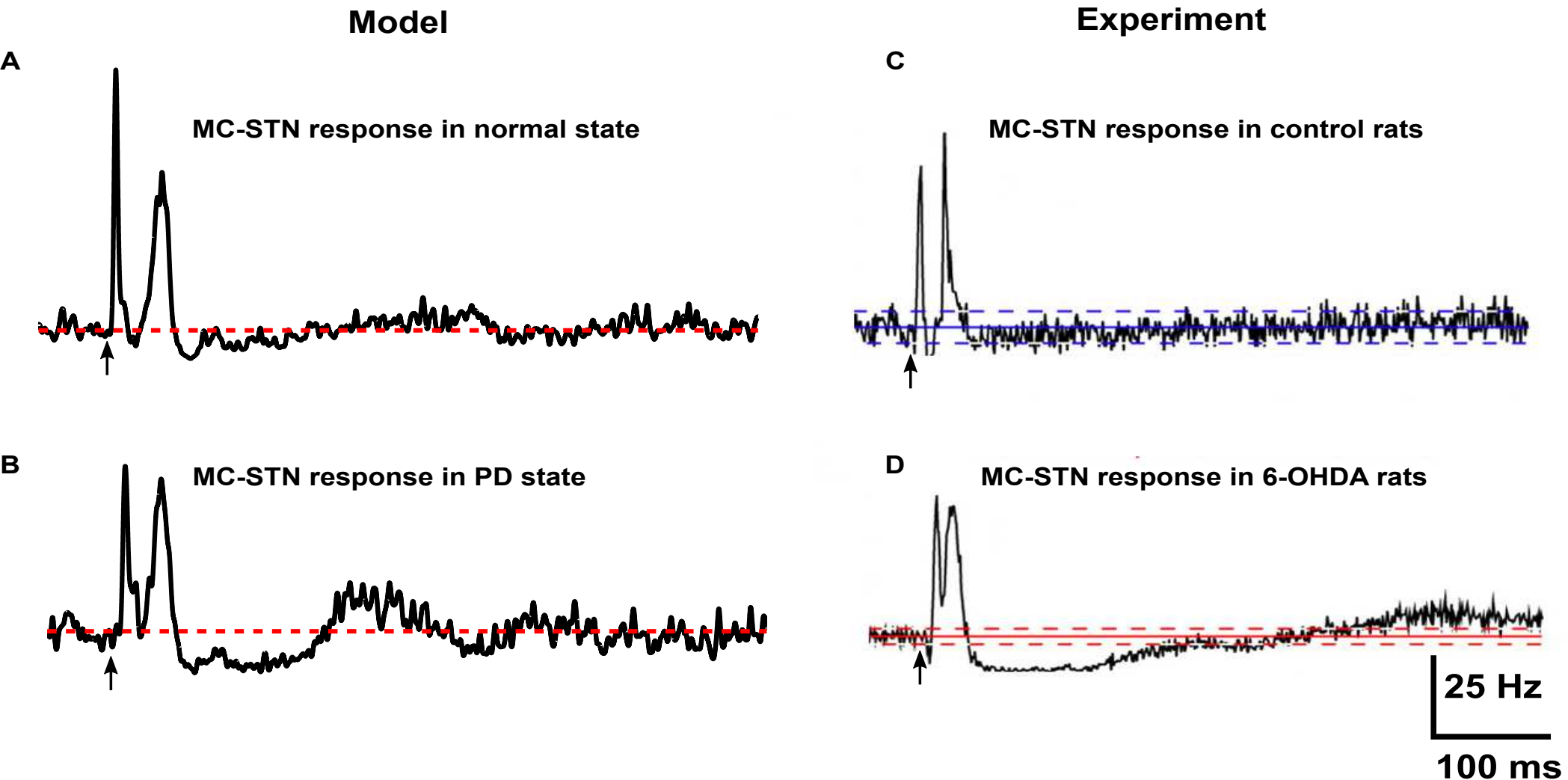
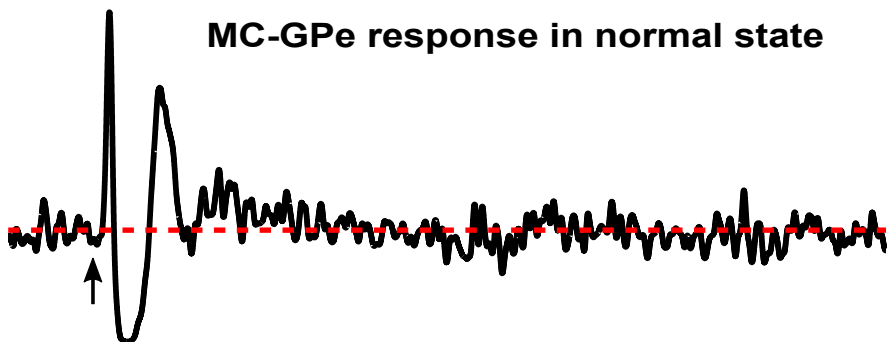


Figure 2

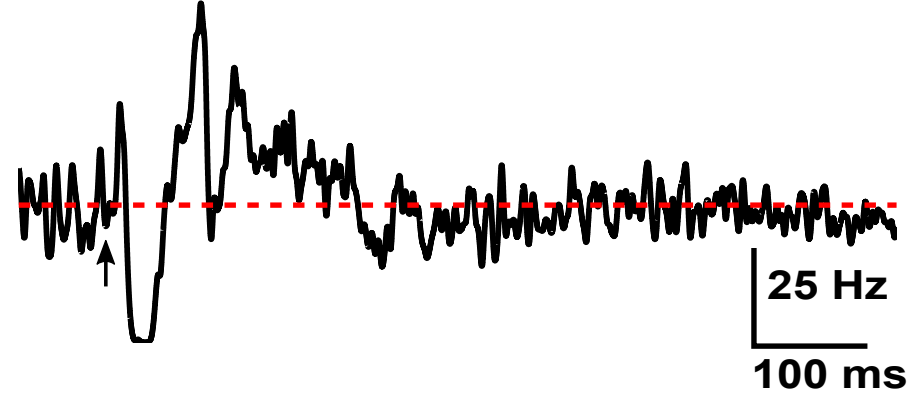
[Click here to download Figure Figure\\_2.eps](#)



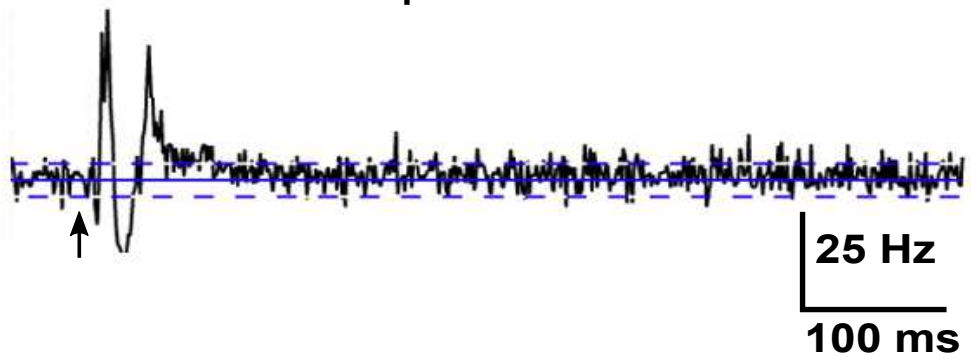
A

**Model****MC-GPe response in normal state**

B

**MC-GPe response in PD state**

C

**Experiment****MC-GPe response in control rats**

D

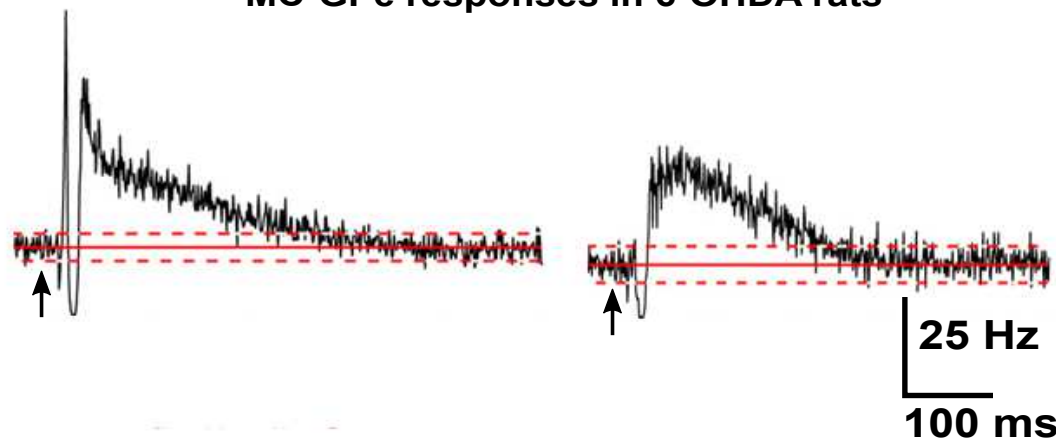
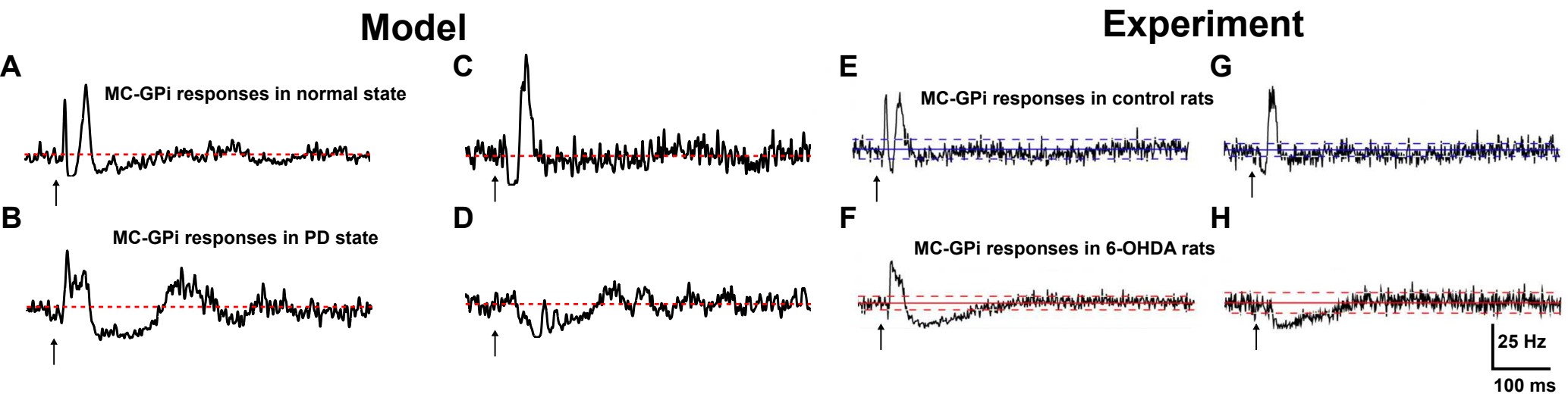
**MC-GPe responses in 6-OHDA rats**

Figure 5

[Click here to download Figure Figure\\_5.eps](#)

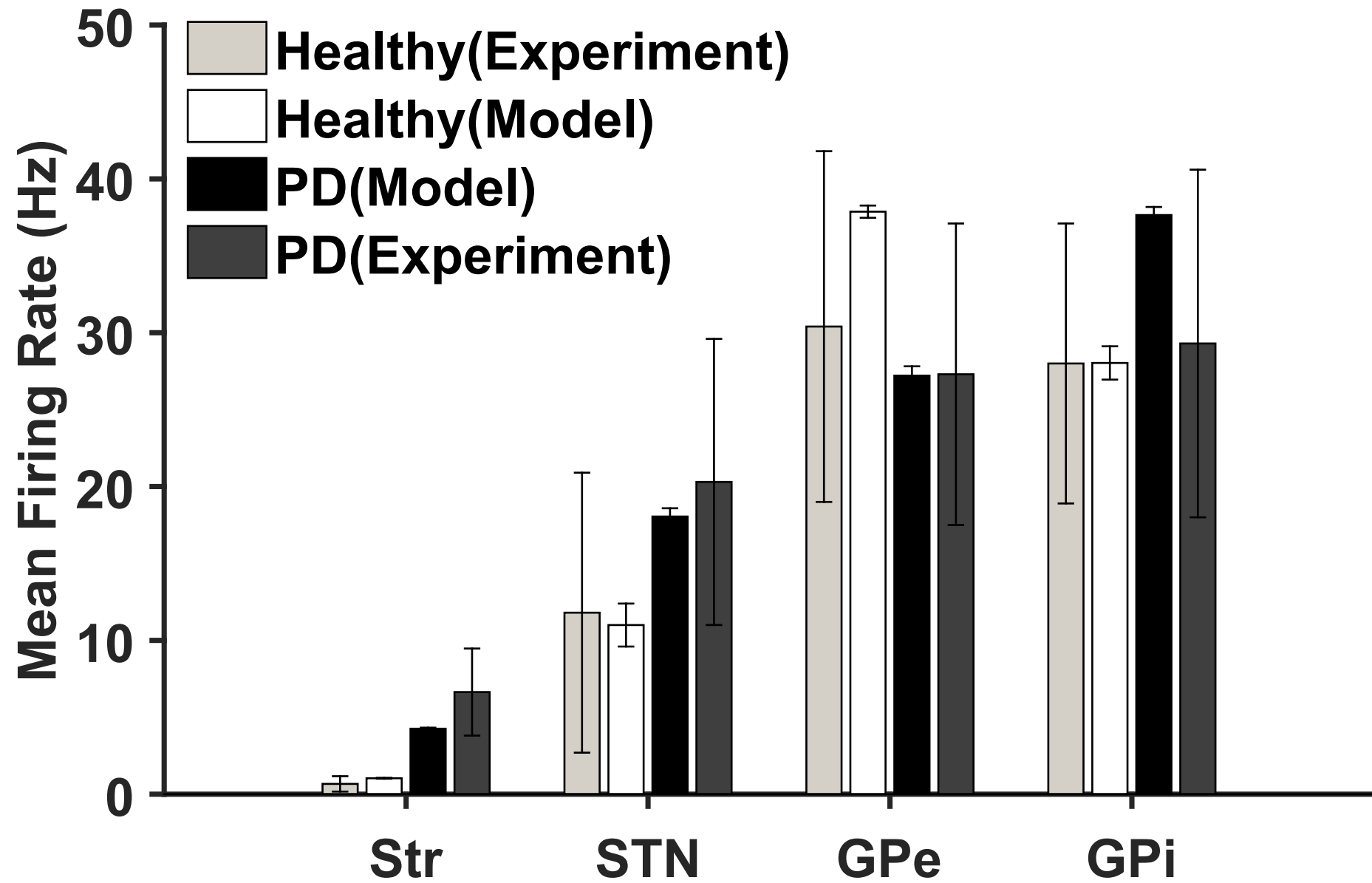


Figure 7

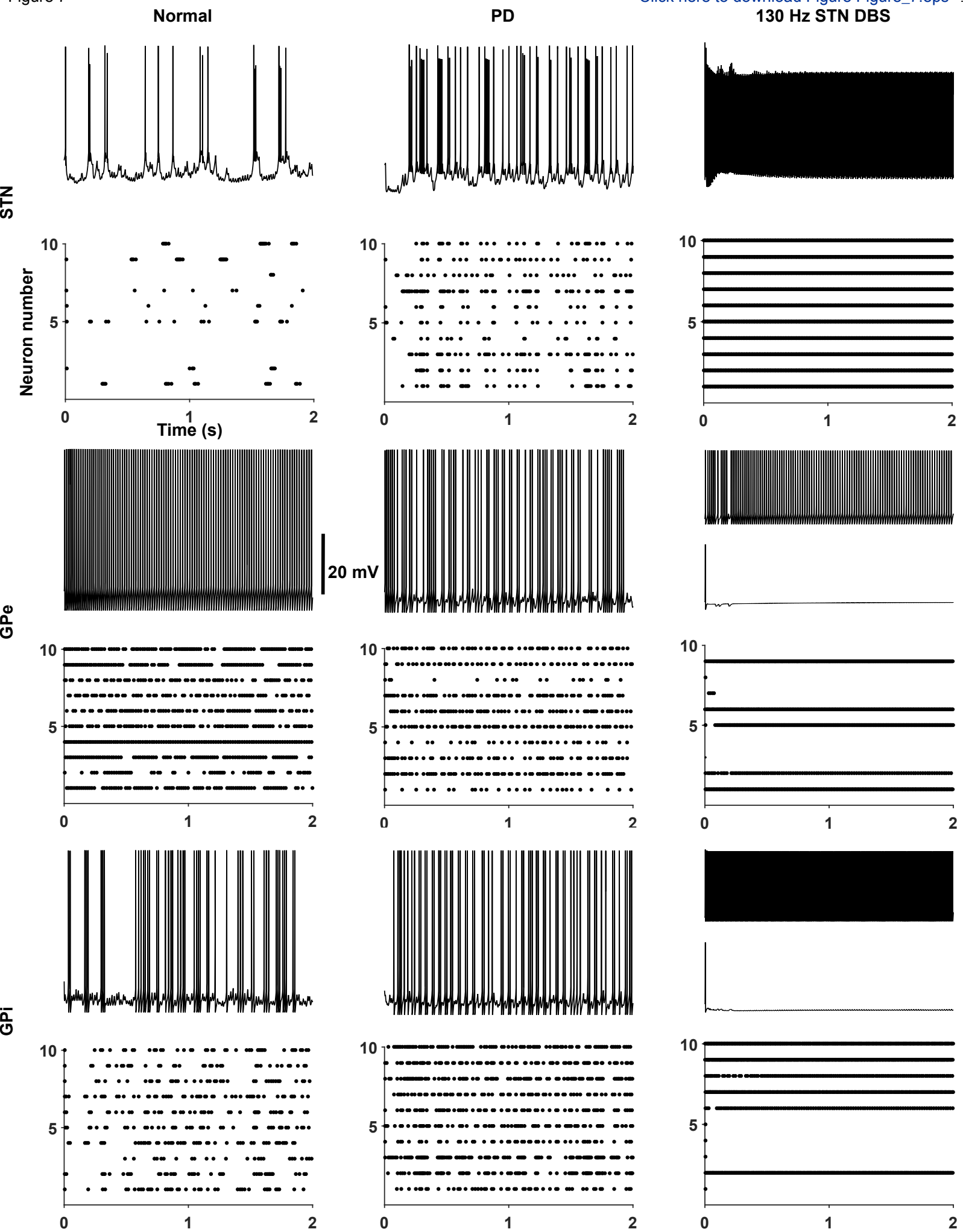
[Click here to download Figure Figure\\_7.eps](#)


Figure 8

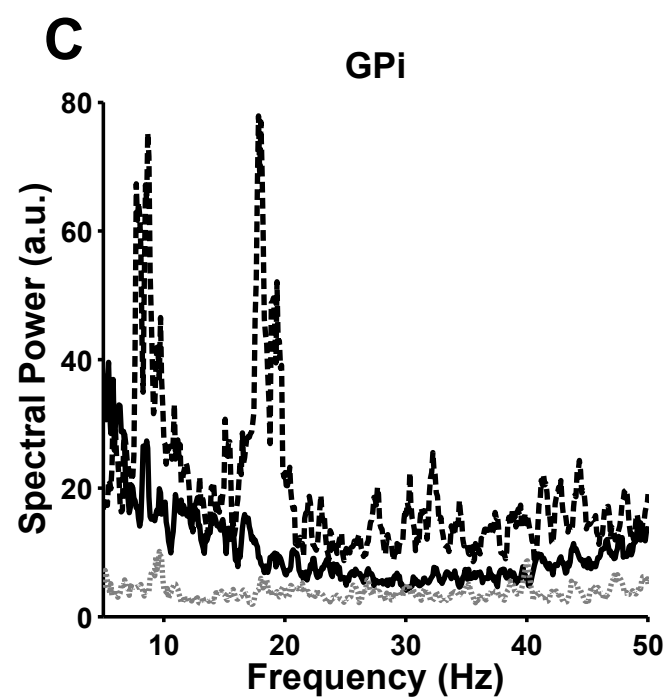
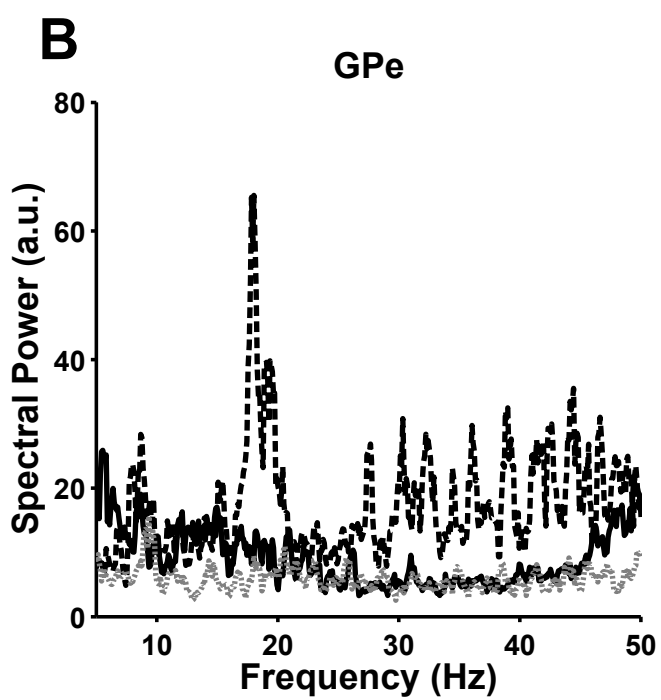
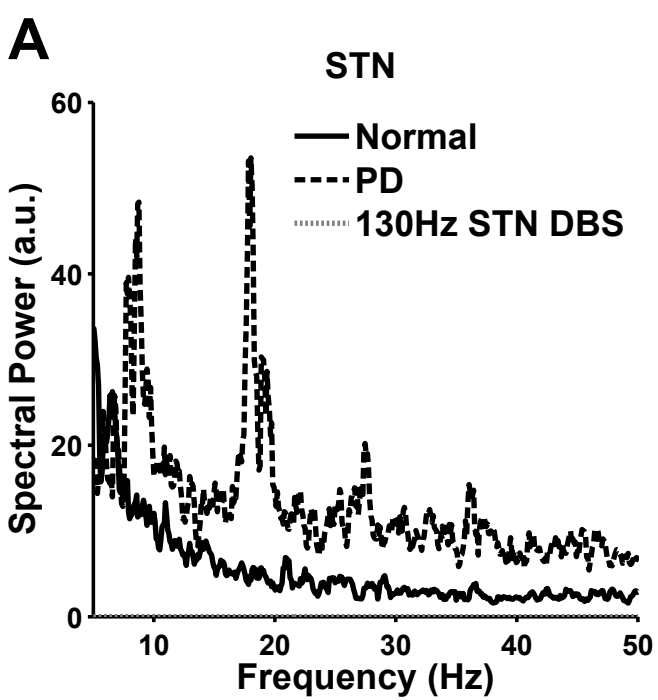
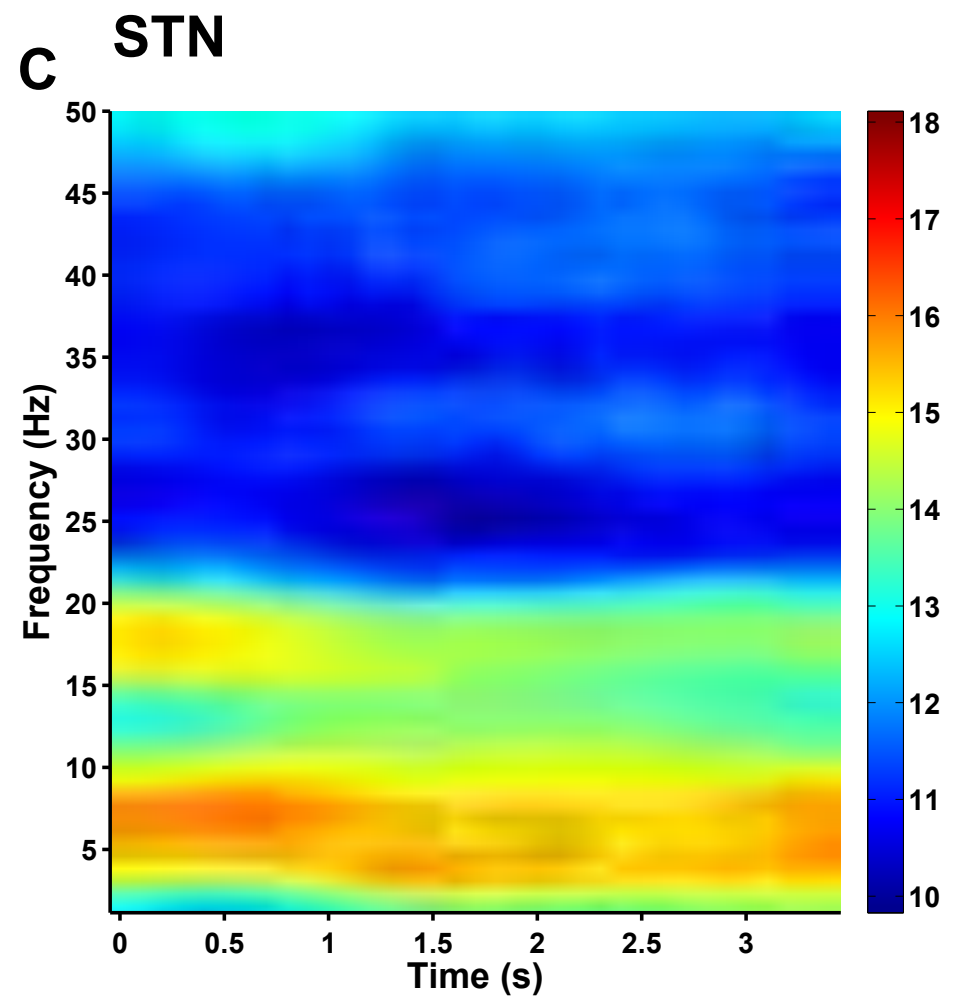
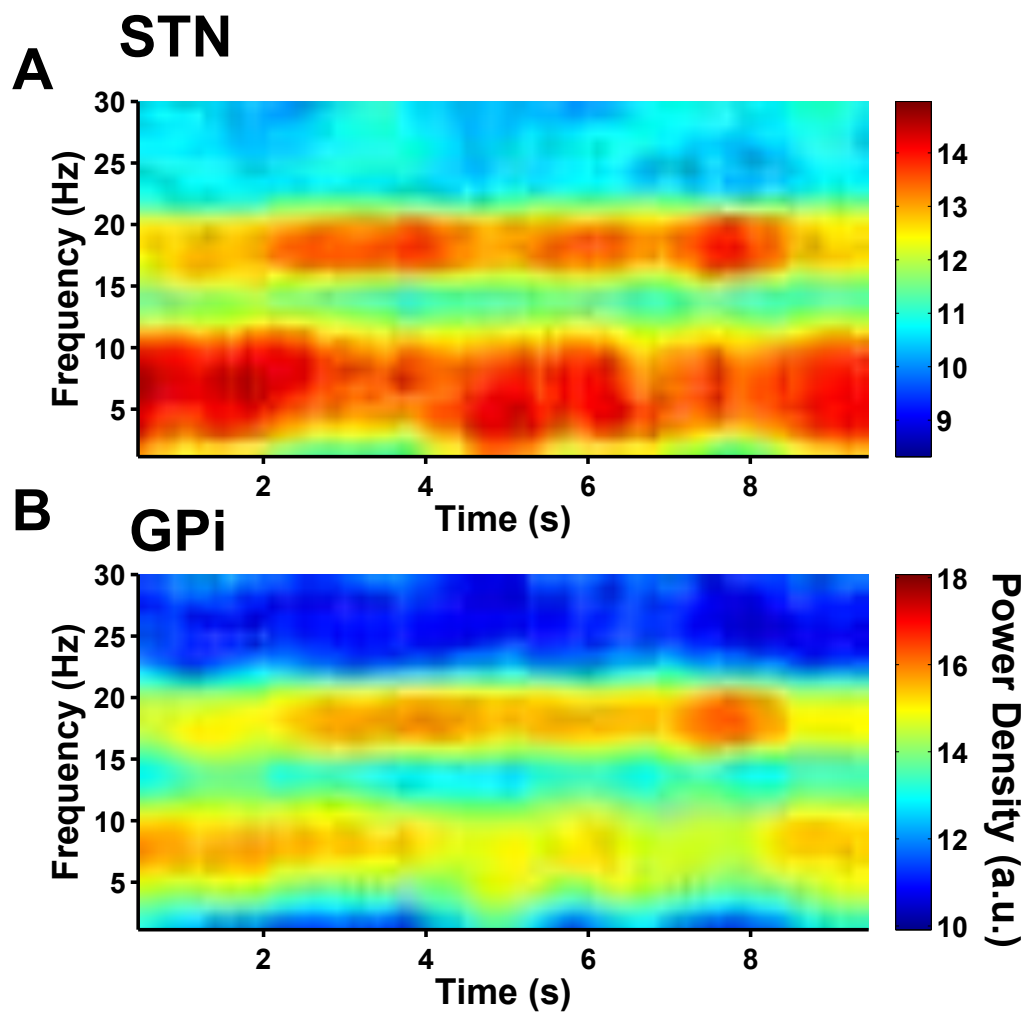
[Click here to download Figure Figure\\_8.eps](#)

Figure 9

[Click here to download Figure Figure\\_9.eps](#)

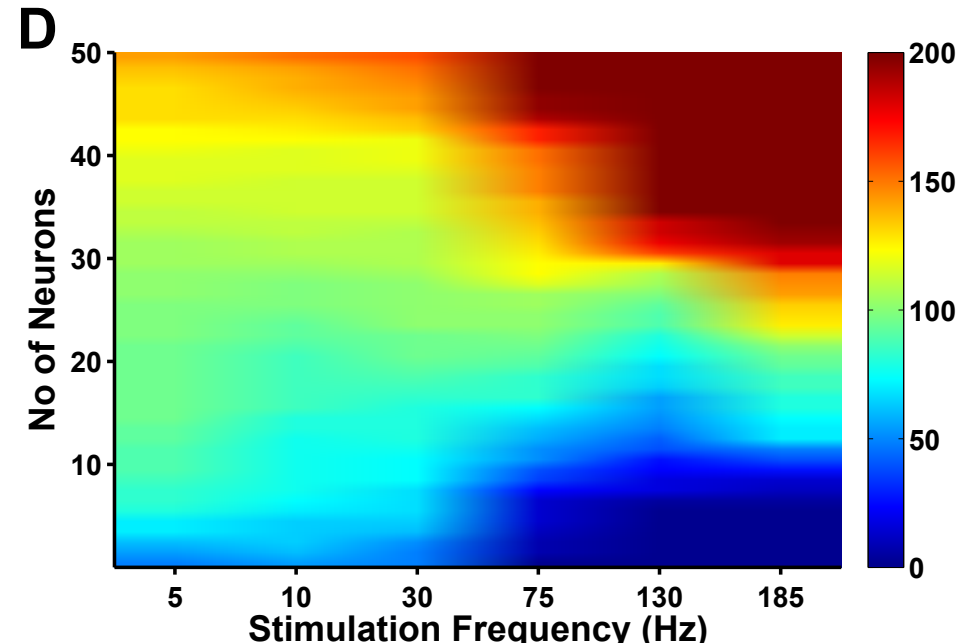
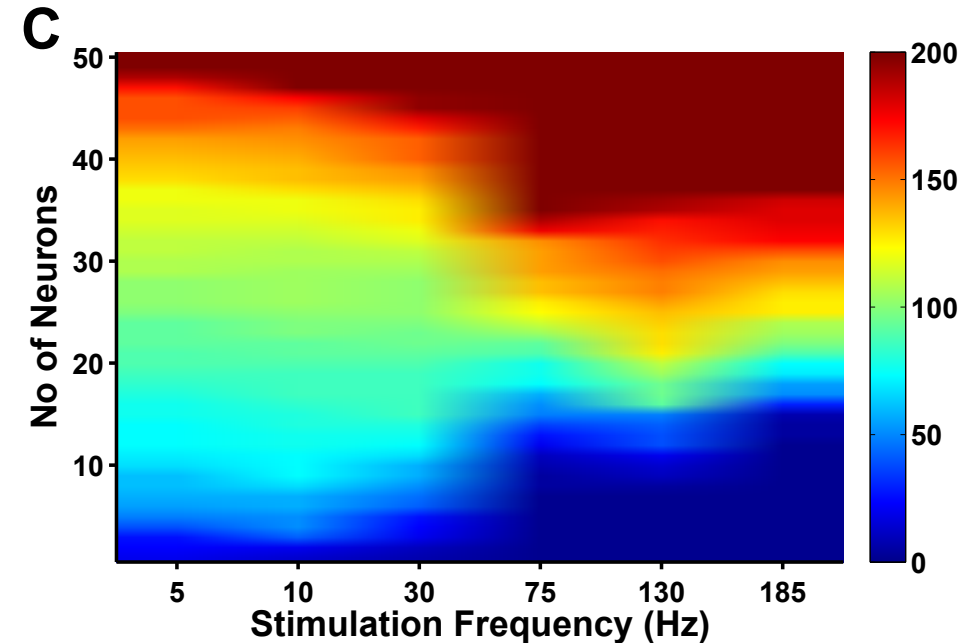
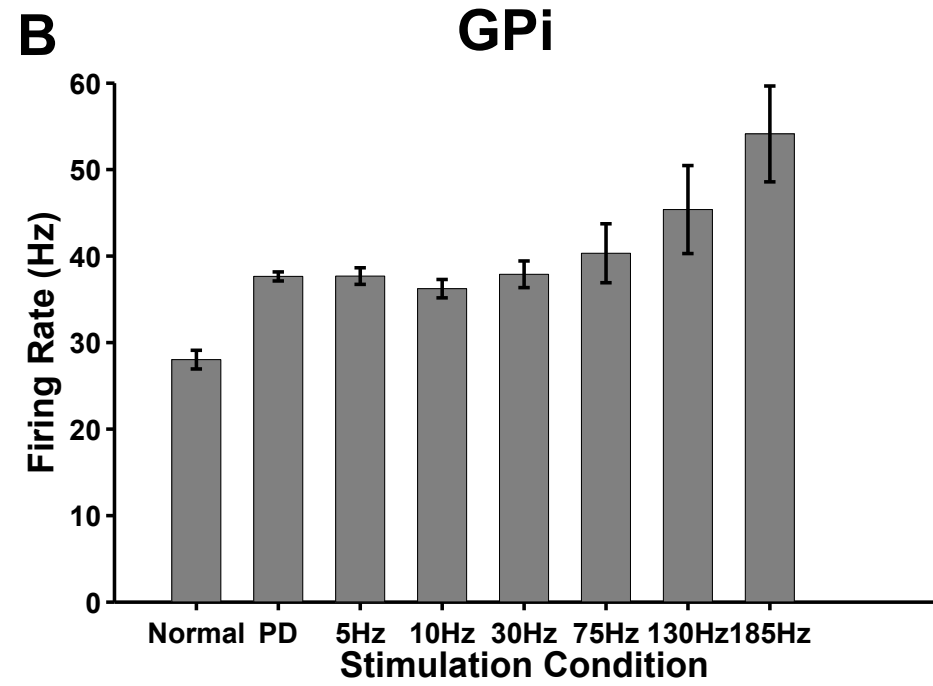
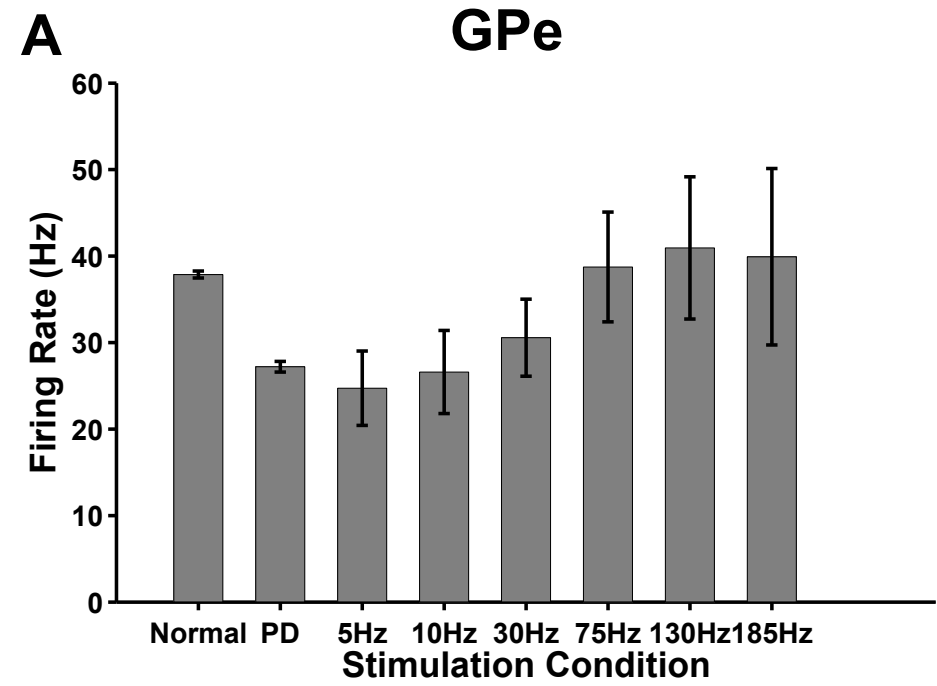


Figure 11

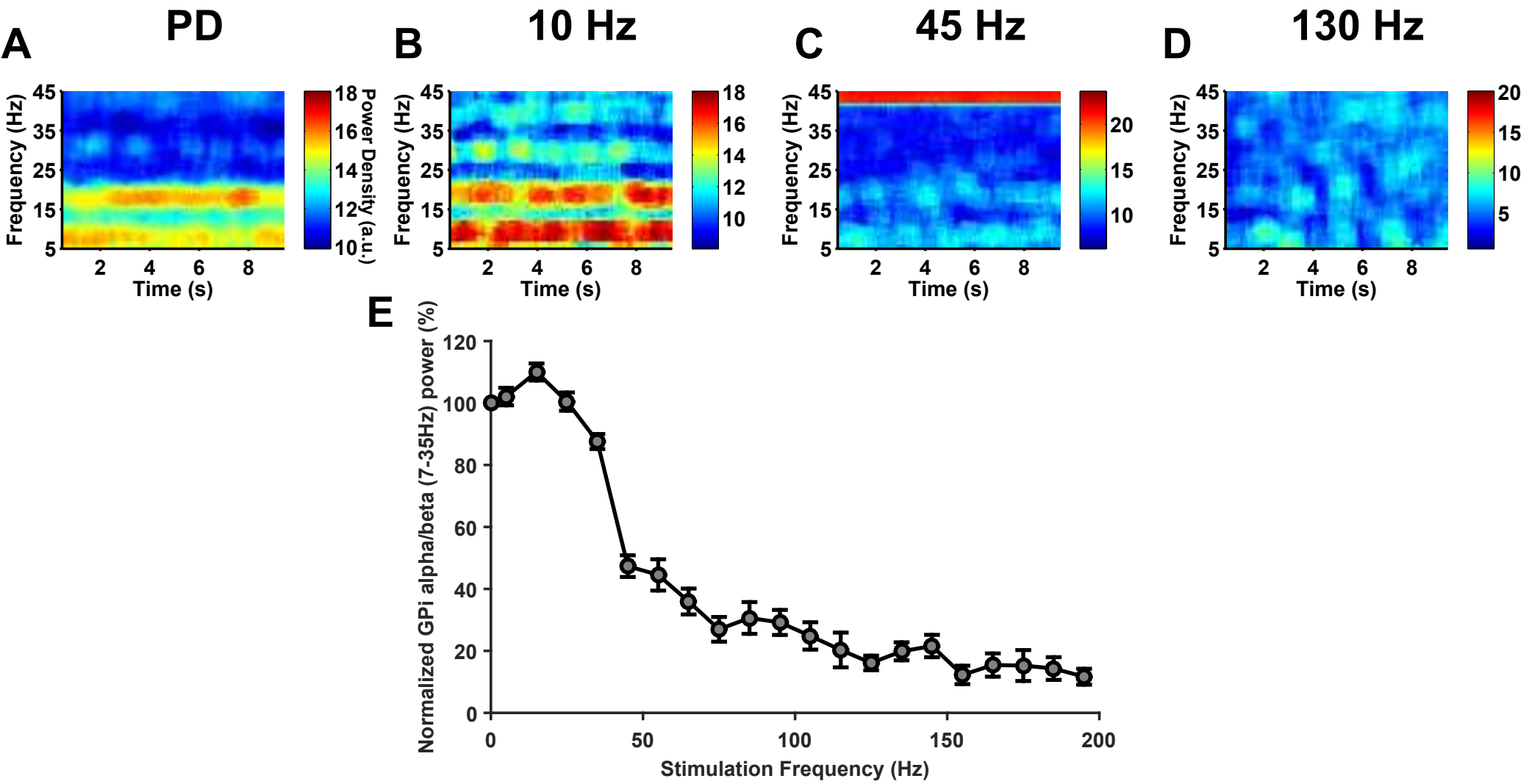
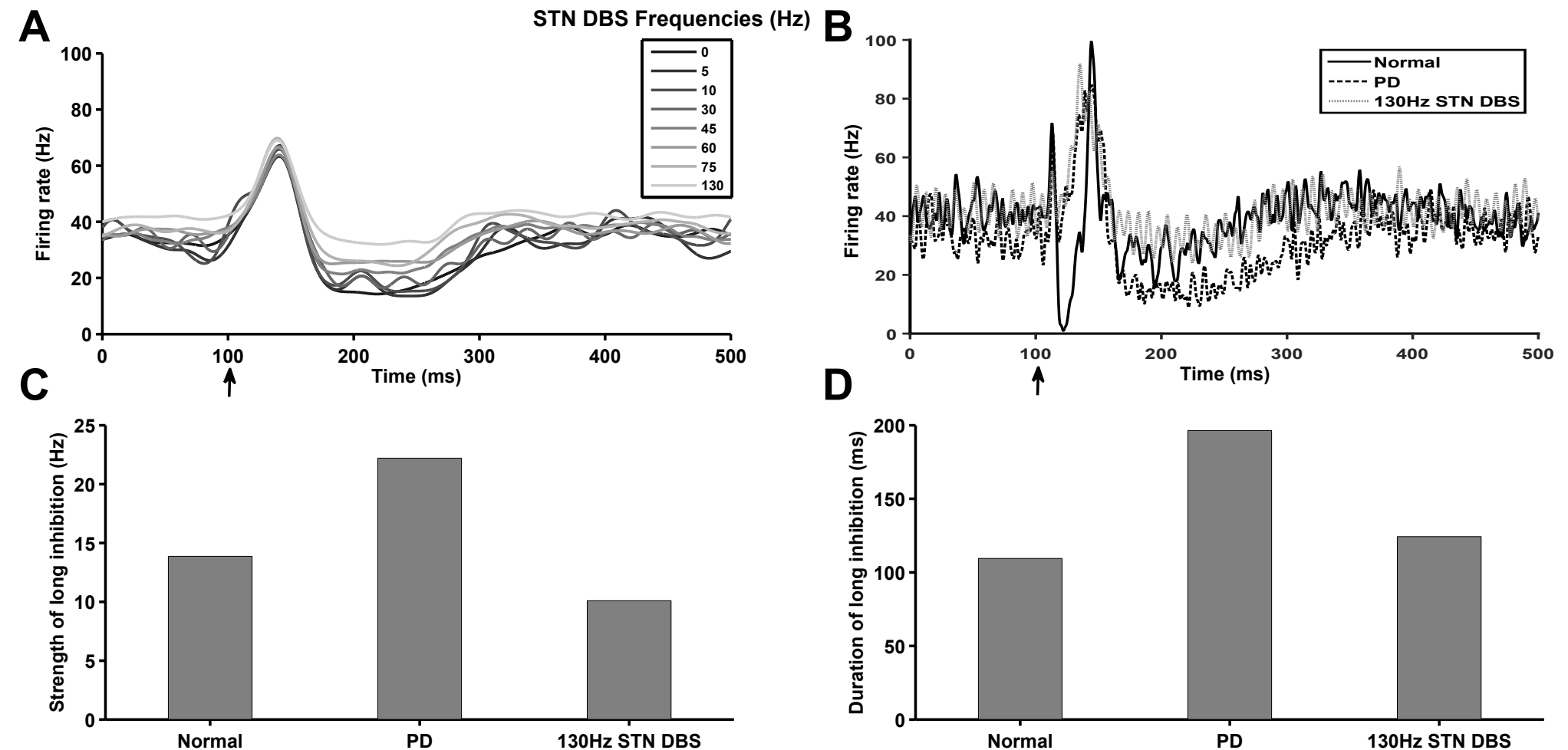
[Click here to download Figure Figure\\_11.eps](#)

Figure 12

[Click here to download Figure Figure\\_12.eps](#)


[Click here to view linked References](#)

1  
2  
3  
4  
5     **A BIOPHYSICAL MODEL OF THE CORTEX-BASAL GANGLIA-THALAMUS**  
6     **NETWORK IN THE 6-OHDA LESIONED RAT MODEL OF PARKINSON'S DISEASE**  
7

8                 Karthik Kumaravelu<sup>1</sup>, David T. Brocker<sup>1</sup>, and Warren M. Grill<sup>1, 2, 3, 4\*</sup>  
9  
10  
11

12     *1 Duke University, Department of Biomedical Engineering, Durham, NC, USA*  
13     *2 Duke University, Department of Electrical and Computer Engineering, Durham, NC, USA*  
14     *3 Duke University, Department of Neurobiology, Durham, NC, USA*  
15     *4 Duke University, Department of Surgery, Durham, NC, USA*  
16

17                 \* Correspondence:  
18  
19

20                 Warren M. Grill, Ph.D.  
21                 Duke University  
22                 Department of Biomedical Engineering  
23                 136 Hudson Hall, Box 90281  
24                 Durham, NC, 27708, USA  
25                 warren.grill@duke.edu  
26                 919 660-5276 Phone  
27                 919 684-4488 FAX  
28  
29  
30  
31  
32

33     **Acknowledgements**  
34

35     This work was supported by grants from the US National Institutes of Health (NIH R37  
36     NS040894 and NIH R01 NS079312). The authors would like to thank the Duke Shared Cluster  
37     Resource team for computational support.  
38  
39  
40  
41  
42  
43  
44  
45  
46  
47  
48  
49  
50  
51  
52  
53  
54  
55  
56  
57  
58  
59  
60  
61  
62  
63  
64  
65

1  
2  
3  
4 **ABSTRACT**  
5  
6  
7  
8  
9  
10  
11  
12  
13  
14  
15  
16  
17  
18  
19  
20  
21  
22  
23  
24  
25  
26  
27  
28  
29  
30  
31  
32  
33  
34  
35  
36  
37  
38  
39  
40  
41  
42  
43  
44  
45  
46  
47  
48  
49  
50  
51  
52  
53  
54  
55  
56  
57  
58  
59  
60  
61  
62  
63  
64  
65

Electrical stimulation of sub-cortical brain regions (the basal ganglia), known as deep brain stimulation (DBS), is an effective treatment for Parkinson's disease (PD). Chronic high frequency (HF) DBS in the subthalamic nucleus (STN) or globus pallidus interna (GPi) reduces motor symptoms including bradykinesia and tremor in patients with PD, but the therapeutic mechanisms of DBS are not fully understood. We developed a biophysical network model comprising of the closed loop cortical-basal ganglia-thalamus circuit representing the healthy and parkinsonian rat brain. The network properties of the model were validated by comparing responses evoked in basal ganglia (BG) nuclei by cortical (CTX) stimulation to published experimental results. A key emergent property of the model was generation of low-frequency network oscillations. Consistent with their putative pathological role, low-frequency oscillations in model BG neurons were exaggerated in the parkinsonian state compared to the healthy condition. We used the model to quantify the effectiveness of STN DBS at different frequencies in suppressing low-frequency oscillatory activity in GPi. Frequencies less than 40 Hz were ineffective, low-frequency oscillatory power decreased gradually for frequencies between 50 Hz and 130 Hz, and saturated at frequencies higher than 150 Hz. HF STN DBS suppressed pathological oscillations in GPe/GPi both by exciting and inhibiting the firing in GPe/GPi neurons, and the number of GPe/GPi neurons influenced was greater for HF stimulation than low-frequency stimulation. Similar to the frequency dependent suppression of pathological oscillations, STN DBS also normalized the abnormal GPi spiking activity evoked by CTX stimulation in a frequency dependent fashion with HF being the most effective. Therefore,

therapeutic HF STN DBS effectively suppresses pathological activity by influencing the activity of a greater proportion of neurons in the output nucleus of the BG.

## Keywords

Deep brain stimulation – Parkinson’s disease – 6-OHDA lesioned rat model – Subthalamic nucleus – Computational model – Pathological oscillatory activity

## 1 INTRODUCTION

Parkinson’s disease (PD) is a neurological disorder caused by degeneration of dopaminergic neurons in the substantia nigra pars compacta (SNc) (Agid et al., 1987; Hornykiewicz, 1998). The primary motor symptoms of PD are rest tremor, akinesia/bradykinesia, rigidity, postural instability and gait disorders (Jankovic et al., 2000; Quinn et al., 1989; Rajput et al., 2008). Levodopa, a dopamine precursor, is used as a first-line therapy for treating PD. However, patients treated with levodopa can develop debilitating dyskinesias (Marsden et al., 1982), after which surgical interventions are often recommended. Chronic high frequency stimulation in the subthalamic nucleus (STN) is effective in suppressing PD motor symptoms (Moro et al., 2010; Weaver et al., 2009). However, despite the clinical effectiveness of STN deep brain stimulation (DBS), its mechanisms are not fully understood.

6-OHDA-lesioned rats and MPTP-treated non-human primates are widely used animal models to study the pathophysiology of PD (Blesa & Przedborski, 2014). Although animal models are rendered parkinsonian by a common mechanism (loss of dopaminergic neurons), there is considerable variation in the neuronal activity underlying the pathophysiology, including differences in firing rates, firing patterns, responses to cortical stimulation, and

1  
2  
3  
4 neuronal synchronization across different basal ganglia (BG) structures (Kita & Kita, 2011;  
5  
6 Nambu et al., 2000). Computational models of the BG also play an important role in helping to  
7  
8 understand both the PD pathophysiology and the therapeutic mechanism of DBS. Neural  
9 activity in several existing computational models of the BG closely matches neural acitivity in  
10 MPTP-treated primates (Kang & Lowery, 2013; Rubin & Terman, 2004; So, Kent, et al., 2012),  
11  
12 but no current computational model adequately represents the 6-OHDA rat model of PD.  
13  
14

15 The objective of the present study was to develop a computational model representing  
16 the parkinsonian state in 6-OHDA lesioned rats, and, following validation, use the model to  
17 investigate the therapeutic mechanisms of STN DBS in alleviating parkinsonian symptoms. We  
18 implemented a biophysical model with Hodgkin-Huxley type neurons to represent the closed  
19 loop cortex-basal ganglia-thalamus-cortex circuit, and used the model to study the  
20 effectiveness of STN DBS at different frequencies in suppressing pathological low-frequency  
21 oscillatory neural activity. Pathological low-frequency oscillatory activity across different BG  
22 nuclei is correlated with motor symptoms of Parkinson's disease (Brocke et al., 2013; Kühn et  
23 al., 2008; Levy et al., 2002), and thereby serves as a model-based proxy for the efficacy of DBS.  
24  
25  
26  
27  
28  
29  
30  
31  
32  
33  
34  
35  
36  
37  
38  
39  
40  
41  
42  
43  
44  
45

## 46 2 METHODS

47

48 The model included 10 single compartment model neurons in each of the cortex (CTX),  
49 striatum (Str), STN, globus pallidus externa (GPe), globus pallidus interna (GPI; or, in the rat, the  
50 homologous entopeduncular nucleus, EP), and thalamus (TH) interconnected with model  
51 synapses to form a functional network (Fig. 1(A),(B)). Simulations were implemented in Matlab  
52  
53  
54  
55  
56  
57  
58  
59  
60  
61  
62  
63  
64  
65

R2014a with equations solved using the forward Euler method with a time step of 0.01 ms. All equations are provided in Appendix A.

## 2.1 CTX Model Neuron

The cortical network was comprised of reciprocally connected regular spiking (RS) excitatory neurons and fast-spiking inhibitory interneurons (FSI), both based on the model developed by Izhikevich (Izhikevich, 2003). The membrane potential,  $v_{rs}$ , of a regular spiking cortical neuron was calculated using

$$\frac{dv_{rs}}{dt} = 0.04 * v_{rs}^2 + 5 * v_{rs} + 140 - u_{rs} - I_{ie} - I_{thco}$$

where  $I_{ie}$  is the synaptic current from FSI to RS neuron (each RS neuron received synaptic input from four randomly selected FSI), and  $I_{thco}$  is the synaptic input received from the TH (each RS neuron received synaptic input from a single TH neuron). An alpha synapse was used to model the synaptic dynamics,

$$S = \bar{g}_{syn} * \frac{t - t_d}{\tau} * e^{-\frac{t-t_d}{\tau}}$$

where  $\bar{g}_{syn}$  is the maximal synaptic conductance,  $t_d$  is the synaptic transmission delay, and  $\tau$  is the time constant. All synaptic transmission delays are shown in Table 1.

The membrane potential,  $v_{fsi}$ , of a FSI was calculated using

$$\frac{dv_{fsi}}{dt} = 0.04 * v_{fsi}^2 + 5 * v_{fsi} + 140 - u_{fsi} - I_{ei}$$

where  $I_{ei}$  is the synaptic current from RS to FSI neuron (each FSI received synaptic inputs from four randomly selected RS neurons). In both equations,  $u$  is a state variable that represents the recovery of membrane potential.

1  
2  
3  
4     **2.2 Str Model Neuron**  
5  
6  
7  
8  
9  
10  
11  
12  
13  
14  
15  
16  
17  
18  
19  
20

Medium spiny neurons (MSN) comprise 90-95% of all striatal neurons in rodents (Chang & Kitai, 1985; Chang et al., 1982), and MSN neurons of the direct and indirect pathways are modulated by D1 and D2 dopamine receptors, respectively (Nicola et al., 2000). The striatal network included medium spiny neurons (MSN) from both the direct and indirect pathways, as developed previously (McCarthy et al., 2011). The membrane potential  $v_{str}$  of direct and indirect MSNs was calculated using

22      $C_m \frac{dv_{str}}{dt} = -I_l - I_K - I_{Na} - I_m - I_{gaba} - I_{costr}$   
23  
24

where  $I_{Na}$ ,  $I_K$  and  $I_l$  are voltage-dependent sodium and potassium ionic currents and a non-specific leakage current,  $I_m$  is an outward potassium current modulated by acetylcholine through M1 muscarinic receptors, and  $I_{gaba}$  is recurrent inhibitory synaptic current (each direct and indirect MSNs received inhibitory axonal collaterals from 30% and 40% of the remaining MSNs, respectively (Taverna et al., 2008), modeled using an exponential synapse), and  $I_{costr}$  is the synaptic input from the CTX (each MSN received excitatory input from one RS CTX neuron, modeled using an alpha synapse). The exponential synapse was modeled using

44      $S = \bar{g}_{syn} * e^{-\frac{t-t_d}{\tau}}$   
45  
46

where  $\bar{g}_{syn}$  is the maximal synaptic conductance,  $t_d$  is the synaptic transmission delay, and  $\tau$  is the time constant.

51     **2.3 STN Model Neuron**  
52  
53

STN neurons were adopted from a previous model (Otsuka et al., 2004) and were spontaneously active with firing rates in the range of 2-10 Hz, which is comparable to rates observed in rat *in vivo*. The membrane potential of a STN neuron,  $v_{stn}$ , was calculated using

$$C_m \frac{dv_{STN}}{dt} = -I_{Na} - I_K - I_a - I_L - I_T - I_{CaK} - I_l - I_{gesn} - I_{cosn,amp} - I_{cosn,nmda} + I_{dbs}$$

where  $I_{Na}$ ,  $I_K$ , and  $I_l$  are voltage-gated sodium and potassium ionic currents and a non-specific leakage current,  $I_L$  is a L-type calcium current,  $I_T$  is a T-type calcium current,  $I_{CaK}$  is a calcium-dependent potassium current that is dependent upon the intracellular calcium concentration, and  $I_{gesn}$  is the inhibitory synaptic current from GPe with dynamics modeled using a bi-exponential synapse,

$$t_p = t_d + \frac{\tau_d * \tau_r}{\tau_d - \tau_r} * \ln \frac{\tau_d}{\tau_r}$$

$$f = \frac{1}{-e^{-\frac{(t_p-t_d)}{\tau_r}} + e^{-\frac{(t_p-t_d)}{\tau_d}}}$$

$$S = \bar{g}_{syn} * f * (e^{-\frac{t-t_d}{\tau_d}} - e^{-\frac{t-t_d}{\tau_r}})$$

Here,  $\bar{g}_{syn}$  is the maximal synaptic conductance,  $t_d$  is the synaptic transmission delay,  $\tau_r$  is the rise time, and  $\tau_d$  is the decay time. Rise and decay times of  $\tau_r = 1.1\text{ ms}$  and  $\tau_d = 7.8\text{ ms}$  respectively were used for IPSCs elicited at GPe-STN synapses (Baufreton et al., 2009). Each STN neuron received inhibitory input from two GPe neurons. Model STN neurons included both AMPA and NMDA glutamate receptors with the AMPA/NMDA receptor ratio equal to one (Farries et al., 2010).  $I_{cosn,amp}$  and  $I_{cosn,nmda}$  are the CTX-STN synaptic currents mediated by AMPA-R and NMDA-R, respectively (each STN neuron received excitatory input from two cortical neurons). Rapid rise ( $\tau_r = 0.5\text{ ms}$ ) and decay ( $\tau_d = 2.49\text{ ms}$ ) times were used for AMPA-R EPSCs, while NMDA-R EPSCs ( $\tau_r = 2\text{ ms}$  and  $\tau_d = 90\text{ ms}$ ) were kinetically slower.

## 2.4 GP Model Neurons

The GPe and GPi/EP neurons were modified from those in a previous model (So, Kent, et al., 2012). The constant applied bias current representing the striatal input to GPe was replaced

1  
2  
3  
4 by the synaptic current from indirect MSNs. The membrane potential of a GPe neuron,  $v_{GPe}$ ,  
5  
6 was calculated using  
7  
8

9

$$C_m \frac{dv_{GPe}}{dt} = -I_l - I_K - I_{Na} - I_T - I_{Ca} - I_{ahp} - I_{sng,e,amp} - I_{sng,e,nmd} - I_{geg,e} - I_{strgpe} + I_{appgpe}$$

10  
11  
12  
13  
14  
15  
16  
17  
18  
19  
20  
21  
22  
23  
24  
25  
26  
27  
28  
29  
30  
31  
32  
33  
34  
35  
36  
37  
38  
39  
40  
41  
42  
43  
44  
45  
46  
47  
48  
49  
50  
51  
52  
53  
54  
55  
56  
57  
58  
59  
60  
61  
62  
63  
64  
65

The ionic currents are similar to STN neurons, as described above, except for the addition of a high threshold calcium current,  $I_{Ca}$ , and the absence of a L-type calcium current. Pallidal neurons receive differential innervation from STN and this is believed to be the origin of the dichotomous firing behavior of GP neurons in rodents (Mallet, Pogosyan, Márton, et al., 2008). Consistent with this observation, the model included two types of GPe neurons, with some receiving excitatory input from two STN neurons ( $I_{sng,e,amp}$  and  $I_{sng,e,nmd}$ ), while others did not (Fig. 1(B)). The STN-GPe synaptic connections were mediated by both AMPA and NMDA glutamate receptors (Götz et al., 1997). The decay time of GPe NMDA-R was slightly faster ( $\tau_d = 67\text{ ms}$ ) when compared to STN NMDA-R, although the rise times were identical in both neurons. The kinetics of GPe AMPA-R were identical to STN. All GPe neurons received inhibitory axonal collateral from two other GPe neurons ( $I_{geg,e}$ ) (Bolam et al., 2000). Each GPe neuron received inhibitory input from all indirect Str MSNs, and these accounted for nearly 80-90% of the total synaptic connections found in GPe (Sims et al., 2008). GPe neurons received an applied bias current  $I_{appgpe}$  ( $3\text{ }\mu\text{A}/\text{cm}^2$ ).

GPi (or, entopeduncular nucleus, EP) is the primary output nucleus of the BG. The membrane potential,  $v_{GPi}$ , of a GPi neuron was calculated using

$$C_m \frac{dv_{GPi}}{dt} = -I_l - I_K - I_{Na} - I_T - I_{Ca} - I_{ahp} - I_{sng,i,amp} - I_{geg,i} - I_{strgpi} + I_{appgpi}$$

with ionic currents similar to GPe neurons described above.  $I_{gegi}$ ,  $I_{strgpi}$  and  $I_{sngi,amp}$  are the synaptic inputs from GPe, direct Str MSN, and STN, respectively, all converging onto GPi neurons (Kita, 2001). Each GPi neuron received inhibitory input from two GPe neurons ( $I_{gegi}$ ) and from all direct Str MSNs ( $I_{strgpi}$ ). STN-GPi synaptic connectivity was similar to GPe with a portion of GPi neurons not receiving any synaptic input from STN (Fig. 1(B)). However, STN-GPi synaptic dynamics were mediated by only AMPA-R with kinetics identical to those of STN-GPe. GPi neurons also received an applied bias current  $I_{appgpi}$  ( $3 \mu A/cm^2$ ).

## 2.5 TH Model Neuron

TH neurons were modified from those in a previous model (So, Kent, et al., 2012). The current pulses to TH representing the sensorimotor cortical (SMC) input were replaced by a constant applied current ( $I_{appth} = 1.2 \mu A/cm^2$ ) representing the cerebellar input to TH. The membrane potential of a TH neuron,  $v_{Th}$ , was calculated using

$$C_m \frac{dv_{Th}}{dt} = -I_l - I_K - I_{Na} - I_T - I_{gith} + I_{appth}$$

with ionic currents similar to the GPe neurons described above. Each TH neuron received inhibitory input from a single GPi neuron ( $I_{gith}$ ).

**Table 1** Synaptic Connection Parameters

Synaptic connection	Transmission delay ( $t_d$ )	Source
CTX-dStr	5.1 ms	(Kita & Kita, 2011)
CTX-idStr	5.1 ms	(Kita & Kita, 2011)

CTX-STN	5.9 ms	(Kita & Kita, 2011)
dStr-GPi	4 ms	(Nakanishi et al., 1987)
idStr-GPe	5 ms	(Kita & Kitai, 1991)
STN-GPi	1.5 ms	(Nakanishi et al., 1987)
STN-GPe	2 ms	(Kita & Kitai, 1991)
GPe-STN	4 ms	(Fujimoto & Kita, 1993)
GPe-GPi	3 ms	(Nakanishi et al., 1991)
GPi-TH	5 ms	(Xu et al., 2008)
TH-CTX	5.6 ms	(Walker et al., 2012)

## 2.6 Modeling Different States

We modeled three states representing control (normal), 6-OHDA lesioned (PD), and 6-OHDA lesioned plus STN DBS in rats. The PD state, resulting from the loss of striatal dopamine neurons, was implemented by making three changes to the normal state. First, loss of striatal dopamine is accompanied by an increase in acetylcholine levels (Ach) in the Str (Ikarashi et al., 1997). This results in a reduction of M-type potassium current in both the direct and indirect MSNs (Brown, 2010; McCarthy et al., 2011), and was modeled by decreasing the maximal conductance  $g_m$  from 2.6 to  $1.5 \text{ mS/cm}^2$ . Second, dopamine loss results in reduced sensitivity of direct Str MSN to cortical stimulation (Mallet et al., 2006), which was modeled by decreasing the maximal corticostriatal synaptic conductance  $g_{costr}$  from 0.07 to  $0.03 \text{ mS/cm}^2$ . Finally, striatal dopamine depletion causes an increase in the synaptic strength of intra-GPe axonal

1  
2  
3  
4 collaterals resulting in aberrant GPe firing (Miguelz et al., 2012), and this was modeled by  
5  
6 increasing the maximal synaptic conductance  $g_{gege}$  from 0.25 to 0.5  $mS/cm^2$ . DBS was modeled  
7  
8 by applying intracellular current pulses in all STN model neurons so that every pulse evoked one  
9 action potential at frequencies in the range of 5-200 Hz (amplitude 300  $\mu A/cm^2$ , duration  
10  
11 0.3 ms).  
12  
13  
14  
15  
16  
17  
18  
19

## 2.7 Outcome Measures

20 PD is accompanied by an increase in low-frequency oscillatory activity across the cortex  
21  
22 and BG (Mallet, Pogosyan, Márton, et al., 2008; Mallet, Pogosyan, Sharott, et al., 2008;  
23  
24 McConnell et al., 2012). Oscillatory power in the beta band correlates with  
25  
26 akinesia/bradykinesia (Kühn et al., 2008), while oscillations in the alpha band may be associated  
27  
28 with tremor (Shaw & Liao, 2005). Therefore, we quantified the effects of STN DBS at different  
29  
30 frequencies on low-frequency oscillatory power in the model GPi in the PD state. Spectral  
31  
32 analyses were performed using the Chronux neural signal analysis package ([www.chronux.org](http://www.chronux.org))  
33  
34 (sliding 1 s window, 0.1 s step size and [3 5] tapers [3 is the time-bandwidth product and 5 is the  
35  
36 number of tapers]) and MATLAB R2014a. Oscillatory power in the GPi was calculated by  
37  
38 integrating the spectral power of GPi spike times in the 7-35 Hz frequency band. Changes in the  
39  
40 responses evoked in GPi by CTX activation might be associated with PD motor symptoms  
41  
42 (Degos et al., 2005; Kita & Kita, 2011). Therefore, we also quantified the strength and duration  
43  
44 of the GPi response (long inhibition) evoked by CTX stimulation and used it as a surrogate to  
45  
46 study the frequency dependent effects of STN DBS.  
47  
48  
49  
50  
51  
52  
53  
54  
55  
56  
57  
58  
59  
60  
61  
62  
63  
64  
65

1  
2  
3  
4 **3 MODEL VALIDATION**  
5

6 We applied supra-threshold stimulus pulses to each cortical neuron (duration 0.3 ms,  
7 amplitude 300  $\mu$ A/cm<sup>2</sup>, frequency 1 Hz) and analyzed the activity evoked in Str, STN, GPe and  
8 GPi using post-stimulus time histograms (PSTH) in the normal and PD states. The PSTH had a bin  
9 width of 1 ms and was averaged across 10 neurons for 100 trials. The model PSTHs were  
10 compared with experimental results obtained under similar conditions (Kita & Kita, 2011).  
11  
12  
13  
14  
15  
16  
17  
18  
19  
20

21 **3.1 Str Response to CTX Stimulation**  
22

23 CTX stimulation evoked a strong excitatory response in model Str MSNs in both the  
24 normal and PD conditions, similar to evoked responses in rats (Kita & Kita, 2011) (Fig. 2). In the  
25 PD state, CTX stimulation evoked strong excitation in model Str neurons followed by long-  
26 duration GABAergic inhibition due to cortical disinhibition (Fig. 2(B)). Model Str MSNs  
27 exhibited increased firing in the PD state as compared to the normal condition, and this  
28 increase in mean firing rate was also observed in rat MSNs following dopamine depletion  
29 (Mallet et al., 2006; Pang et al., 2001).  
30  
31  
32  
33  
34  
35  
36  
37  
38  
39  
40  
41  
42

43 **3.2 STN Response to Cortical Stimulation**  
44

45 In the normal state, CTX stimulation evoked early excitation followed by late excitation  
46 in model STN neurons (Fig. 3(A)) by activation via the hyperdirect pathway of AMPA-R and  
47 NMDA-R, respectively. The reduction in firing rate between the early and late excitation was  
48 due to the difference in timing between the activation of AMPA-R and NMDA-R rather than  
49 synaptic inhibition. Following CTX stimulation in the PD state, model STN neurons exhibited  
50 early and late excitation followed by protracted inhibition (Fig. 3(B)) due to the increased late  
51 excitation and prolonged inhibition. This change in the temporal profile of STN activity  
52 may contribute to the motor symptoms of PD, such as bradykinesia and rigidity.  
53  
54  
55  
56  
57  
58  
59  
60  
61  
62  
63  
64  
65

1  
2  
3  
4 excitation of GPe leading to late inhibition of STN. The model PSTHs were consistent with the  
5  
6 experimental PSTHs from rats (Kita & Kita, 2011) (Fig. 3(C),(D)).  
7  
8  
9  
10

### 11 **3.3 GPe Response to Cortical Stimulation** 12

13 In the normal state, model GPe neurons responded to CTX stimulation with early  
14  
15 excitation, short inhibition, and weaker late excitation (Fig. 4(A)). The early excitation and short  
16 inhibition were mediated by STN and Str, respectively, while the late excitation was mediated  
17 by both STN and Str. The GPe response to CTX stimulation in the PD state included early  
18  
19 excitation, short inhibition, and large amplitude and long duration late excitation (Fig. 4(B)). The  
20 increased late excitation in the PD state was due to the protracted inhibition of Str MSNs, which  
21 exhibited higher levels of spontaneous activity in the PD state that disinhibited the GPe  
22  
23 neurons. The model results are similar to the GPe responses in rats (Kita & Kita, 2011; Ryan &  
24  
25 Clark, 1991) (Fig. 4(C),(D)).  
26  
27  
28

### 29 **3.4 GPi Response to Cortical Stimulation** 30

31 The responses evoked in Str, GPe, and STN by CTX stimulation converged on GPi  
32  
33 neurons, which exhibited two major response patterns. CTX stimulation generated either early  
34 excitation, short inhibition, and late excitation or short inhibition followed by late excitation in  
35 model GPi neurons in the normal state (Fig. 5(A),(C)). The early excitation of GPi was due to  
36 activation of STN neurons via the hyperdirect pathway, the short inhibition was mediated by  
37 the activation of direct MSNs, and the late excitation was mediated by the indirect activation of  
38 MSN through GPe and the subsequent disinhibition of GPi. A model GPi neuron exhibited either  
39  
40

1  
2  
3  
4 one of the response types depending upon the strength of synaptic connection it received from  
5  
6 STN neurons.  
7  
8

9 The response patterns in GPi in the PD state differed considerably from those under  
10 normal conditions. CTX stimulation evoked either early excitation followed by strong, long  
11 duration inhibition or only long duration inhibition in model GPi neurons (Fig. 5(B),(D)). The  
12 early short inhibition in the normal state was replaced by strong, long duration inhibition. The  
13 absence of short inhibition was due to the reduced sensitivity of direct MSNs to CTX stimulation  
14 following dopamine depletion, while the increased late excitation in GPe and increased long  
15 inhibition in STN resulted in strong, long duration inhibition in GPi. The model results are similar  
16 to GPi responses measured in rats (Kita & Kita, 2011) (Fig. 5(E),(F),(G),(H)).  
17  
18  
19  
20  
21  
22  
23  
24  
25  
26  
27  
28  
29  
30  
31  
32

### 3.5 Model Neuron Firing Rates and Patterns

33 Recordings in 6-OHDA lesioned rats indicate that there is an increase in Str MSN firing  
34 rate after administration of 6-OHDA (Kita & Kita, 2011; Pang et al., 2001). Similarly, the firing  
35 rates of STN and GPi neurons in 6-OHDA rats are higher than in control, while those of GPe  
36 neurons are lower following lesion (Albin et al., 1989; DeLong, 1990; Hollerman & Grace, 1992;  
37 Mallet, Pogosyan, Márton, et al., 2008). Changes in firing rates of neurons in the model were  
38 consistent with these experimental results (Fig. 6): Str, STN and GPi neurons exhibited  
39 increased firing rates in the PD condition, while GPe neuron firing rates decreased. In the PD  
40 state, the model STN, GPe and GPi neurons exhibited more rhythmic burst-like firing patterns  
41 (Fig. 7), and this was consistent with experimental studies (Kita & Kita, 2011; Mallet, Pogosyan,  
42 Márton, et al., 2008).  
43  
44  
45  
46  
47  
48  
49  
50  
51  
52  
53  
54  
55  
56  
57  
58  
59  
60  
61  
62  
63  
64  
65

## 4 RESULTS

The validated model was used to study the effects of PD and STN DBS on spiking and oscillatory activity of model BG neurons.

#### 4.1 Low-Frequency Oscillatory Activity

Model BG neurons exhibited increased oscillatory activity in the beta band (~ 20Hz) in the PD state when compared to normal conditions (Fig. 8), in agreement with experimental observations following unilateral 6-OHDA lesion (Cruz et al., 2012). The model STN and GPi neurons also exhibited low-frequency oscillatory activity in the alpha band (~ 9 Hz) in the PD condition (Fig. 8), similar to oscillatory activity (7-10 Hz) in 6-OHDA lesioned rats (McConnell et al., 2012). Spectral analysis of the spike times of model BG neurons revealed that episodes of alpha band oscillatory activity interrupted beta oscillatory activity in the PD state (Fig. 9(A),(B)), consistent with experimental evidence that episodes of tremor oscillation desynchronize beta activity in PD patients (Levy et al., 2002).

Infusion of an NMDA antagonist (*cis*-4-[phosphomethyl]-piperidine-2-carboxylic acid) into STN suppressed STN beta band oscillations in 6-OHDA lesioned rats (Pan et al., 2014). Infusion of NMDA antagonist into STN was simulated in the model by reducing the NMDA-R synaptic conductance  $g_{cosn,nmda}$  in the hyperdirect pathway to zero. Similar to the experimental observation, reducing the NMDAR synaptic conductance abolished beta oscillatory activity in model STN neurons, but did not alter low-frequency oscillatory activity (Fig. 9(C)).

## 4.2 Model Neuron Firing Rates during STN DBS

The intrinsic activity of STN neurons was masked during HF STN DBS and firing patterns were more regular (Fig. 7). HF STN DBS resulted in both increases and decreases in the firing

rate of a greater number of model pallidal neurons than low-frequency STN DBS (Fig. 10(C),(D)), consistent with experimental observations in 6-OHDA lesioned rats (McConnell et al., 2012). Excitation through the STN-GPe pathway resulted in increased firing of some GPe neurons, while inhibition through the axonal collaterals of excited GPe neurons reduced the firing rate of other GPe neurons. The increase in GPi firing rate resulted from activation of the STN-GPi pathway, while reductions in rate were due to excitation of GPe neurons and subsequent inhibition of GPi neurons through the STN-GPe-GPi pathway. Due to this dichotomous response, there was no difference in the mean firing rates of the model GPe or GPi neurons at any STN DBS frequency (Fig. 10(A),(B)), matching well the changes in firing rates observed in 6-OHDA lesioned rats during STN DBS (McConnell et al., 2012).

### 4.3 STN DBS Frequency-Dependent Suppression of Beta Frequency Oscillations

Stimulation frequency is a determinant of the effectiveness of STN DBS in reducing PD symptoms in 6-OHDA lesioned rats (So, McConnell, et al., 2012), and abnormal low-frequency oscillatory activity in the output nuclei of the BG is correlated with PD symptoms in the 6-OHDA rat model of PD (McConnell et al., 2012). We quantified the effectiveness of STN DBS in the model by calculating the total low-frequency (7-35Hz) power of activity in model GPi neurons during DBS normalized to the baseline GPi power in the PD state. STN DBS at frequencies less than 40 Hz did not cause any substantial change in the low-frequency power of model GPi neuron activity. The GPi low-frequency power decreased gradually for stimulus frequencies between 50 Hz and 130 Hz, and saturated at stimulation frequencies greater than 150 Hz (Fig. 11). The frequency-dependent suppression of GPi low frequency oscillatory power matched the frequency-dependent suppression of motor symptoms in 6-OHDA rats (Li et al., 2012;

1  
2  
3  
4 McConnell et al., 2012; Ryu et al., 2013). Further, HF STN DBS suppressed low-frequency  
5 oscillations in GPe, STN, and GPi neurons to levels much lower than in the normal and PD states  
6 (Fig. 8(A),(B),(C)).  
7  
8  
9  
10

#### 11 4.4 STN-DBS Frequency-Dependent Normalization of Abnormal GPi Activity Evoked by 12 CTX Stimulation

13  
14

15 Changes in the activity evoked in the BG by CTX might be causative of motor deficits  
16 observed in PD (Degos et al., 2005). In the model during PD conditions, CTX stimulation evoked  
17 abnormal responses in GPi characterized by the absence of early short inhibition present in the  
18 healthy condition and the presence of strong, long-lasting late inhibition not present in the  
19 healthy condition. We quantified the effects of STN DBS on the responses evoked in GPi by CTX  
20 stimulation in the model. STN DBS at frequencies less than 30 Hz did not cause any substantial  
21 change in the GPi response evoked by CTX stimulation (Fig. 12(A)). Both the strength and  
22 duration of late inhibition decreased gradually for stimulus frequencies between 45 Hz and 130  
23 Hz (Fig. 12(A)). During 130Hz STN DBS, the strength and duration of late inhibition in the GPi  
24 response evoked by CTX stimulation in the PD state was greatly normalized (Fig. 12(B),(C),(D)).  
25 However, HF STN DBS did not influence the loss of the early short inhibition in the GPi response  
26 evoked by CTX stimulation under normal conditions (Fig. 12(B)).  
27  
28

## 29 5 DISCUSSION

30  
31

32 We developed a computational model of the cortical-basal ganglia-thalamus circuit in  
33 the 6-OHDA lesioned rat model of PD, including a closed-loop connection between thalamus  
34 and cortex. Following extensive validation, demonstrating that the model replicated a wealth of  
35 experimental data, we used the model to quantify the effects of STN DBS on low-frequency  
36  
37

oscillatory activity. The model was validated by comparing responses evoked by CTX stimulation in Str, STN, GPe, and GPi model neurons with experimental PSTHs. The model accounted for the key differences observed in the response patterns between the normal and PD states. Second, the firing rates and patterns observed in the normal and PD states were consistent with those in experimental studies. Finally, the two key emergent properties of the model – oscillatory activity across different nuclei and stimulation frequency-dependent suppression of this oscillatory activity – also matched well with experimental studies. Finally, the frequency-dependent effects of STN DBS in suppressing pathological low-frequency oscillatory activity paralleled the frequency-dependent normalization of abnormal responses evoked in the output nucleus of the BG by CTX stimulation.

## 5.1 Importance of CTX Induced Responses in GPi

The timing of the GPi response components evoked by CTX stimulation reflects the importance of the direct, indirect and hyperdirect pathways in the normal functioning of the BG. According to the “center-surround model”, the sequence of activation of the three BG pathways is functionally significant (Nambu et al., 2002). When a movement is initiated, the cortex exerts a rapid and strong excitatory influence on the output nucleus of the BG (GPi) via the hyperdirect pathway. Excitation of GPi, which results in inhibition of TH, is thought to negate all competing motor programs. Next, the cortical activation of the direct pathway results in strong inhibition of GPi, which likely disinhibits the TH. This allows the CTX to transmit the selected motor program efficiently through the TH. Finally, the activation of the indirect pathway again causes excitation of the GPi and subsequent inhibition of the TH. The functional implication is believed to be that unwanted motor programs are suppressed, which further aids

in the transmission of only the selected motor program. Nambu and colleagues conducted their study in non-human primates, but the hypotheses they put forward regarding the center-surround model may also apply in rats since the GPi response patterns to CTX stimulation are similar in both the animal models (Kita & Kita, 2011). However, in 6-OHDA lesioned rats, CTX stimulation evokes abnormal responses in GPi with notable differences being the insensitivity of the direct pathway to CTX stimulation and the increased firing of indirect pathway neurons (Kita & Kita, 2011; Mallet et al., 2006). These alterations in the normal functioning of the CTX-BG pathways resulted in abnormal CTX stimulation induced GPi responses in the model. HF STN DBS partially restored the normal functioning of BG pathways in the model by normalizing the abnormal CTX stimulation induced GPi response that a result of increased firing of the indirect pathway neurons. However, HF STN DBS failed to restore the component that was lost as a result of the reduced sensitivity of the direct pathway neurons to CTX stimulation. Hence, we predict in 6-OHDA lesioned rats that increased firing of indirect pathway neurons and transmission of this activity to the BG output nuclei might contribute to PD motor symptoms.

## 5.2 Neural Activity in 6-OHDA Lesioned Rats and Parkinsonian Primates

In both the 6-OHDA-lesioned rat and the MPTP-treated monkey models of PD, striatal dopamine depletion results in an increase in the firing rate of indirect Str MSNs (DeLong, 1990; Mallet et al., 2006; Pang et al., 2001). This is consistent with the classical model of PD that hypothesizes the SNc dopaminergic neurons exert an inhibitory effect on the indirect Str MSN and the loss of this inhibition results in PD symptoms. Also common to both of these animal models is the presence of exaggerated, synchronized pathological low-frequency oscillatory activity across BG nuclei and CTX in the parkinsonian state (Mallet, Pogosyan, Márton, et al.,

1  
2  
3  
4 2008; Raz et al., 2000), and suppression of such activity by effective STN DBS (Hammond et al.,  
5  
6 2007; McConnell et al., 2012). The responses evoked in different BG nuclei by CTX stimulation  
7  
8 are also similar in rats and non-human primates (Kita & Kita, 2011; Nambu et al., 2000;  
9 Tremblay & Filion, 1989). The downstream effects of STN DBS are also similar across the two  
10 species: behaviorally effective STN DBS evokes both excitation and inhibition in both rat and  
11 non-human primate GPi/SNr neurons (Bosch et al., 2011; Dorval et al., 2008; McConnell et al.,  
12 2012).  
13  
14

15 One major difference between the rat and non-human primate models is the firing  
16 rates of BG neurons. The firing rates of STN, GPe, and GPi neurons in rats are much lower when  
17 compared to non-human primates in both normal and parkinsonian conditions (Wichmann &  
18 Soares, 2006). Our model adequately accounts for this difference and the mean firing rate of all  
19 model BG neurons was < 40 Hz in both normal and PD states. The differences in firing rates  
20 likely underlie the variations in the frequency-dependent effects of DBS between the animal  
21 models. While low frequency stimulation (~50 Hz) was sufficient to mask and regularize the  
22 intrinsic activity of a model neuron firing at a low rate, higher frequency stimulation (>100 Hz)  
23 was necessary to achieve similar effects in a neuron that fired at a higher rate (Grill et al., 2004).  
24 In primates, STN DBS frequencies above 100 Hz relieve symptoms, while frequencies below 50  
25 Hz are usually ineffective (Fogelson et al., 2005; Timmermann et al., 2004). However, in rats,  
26 the therapeutic window of STN-DBS starts as low as 50 Hz and reaches peak effectiveness at  
27 around 130 Hz (Li et al., 2012; Ryu et al., 2013). The STN DBS frequency tuning profile in the  
28 model was similar to these experimental studies in rats.  
29  
30  
31  
32  
33  
34  
35  
36  
37  
38  
39  
40  
41  
42  
43  
44  
45  
46  
47  
48  
49  
50  
51  
52  
53  
54  
55  
56  
57  
58  
59  
60  
61  
62  
63  
64  
65

1  
2  
3  
4 **5.3 Prior Computational Models of the BG Circuit**  
5  
6  
7  
8  
9  
10  
11  
12  
13  
14  
15  
16  
17  
18  
19  
20  
21  
22  
23  
24  
25  
26  
27  
28  
29  
30  
31  
32  
33  
34  
35  
36  
37  
38  
39  
40  
41  
42  
43  
44  
45  
46  
47  
48  
49  
50  
51  
52  
53  
54  
55  
56  
57  
58  
59  
60  
61  
62  
63  
64  
65

Efforts continue to understand better the therapeutic mechanism of STN DBS using computational models of the BG. Initial attempts to explain the therapeutic mechanism of HF STN DBS used the classical rate model of PD (Albin et al., 1989). According to this model, dopamine depletion results in an imbalance characterized by decreased activation of the direct pathway and an increased activation of the indirect pathway. Increased activation of the indirect pathway leads to a decrease in GPe firing rate and a subsequent increase in the STN and GPi firing rates. The firing rate of GPi is further increased by the decreased activation of the direct pathway. Therefore, a hyperactive GPi during PD increases inhibition of the TH, which results in bradykinesia/akinesia. Single unit recordings across BG nuclei in 6-OHDA rat and MPTP-treated monkey support the classical rate model (Bergman et al., 1994; Hollerman & Grace, 1992; Mallet, Pogosyan, Márton, et al., 2008; Wichmann & Soares, 2006). However, the classical rate model failed to explain the therapeutic mechanism of STN DBS. Results from experimental studies suggest that DBS activates the efferent axons of the stimulated nucleus (Anderson et al., 2003; Hashimoto et al., 2003). Hence, HF STN DBS should increase the firing rate of GPi neurons. However, according to the classical rate model, a hyperactive GPi during HF STN DBS should lead to a more bradykinetic state than those observed during PD. This prediction of the rate model is in contrast with the clinical outcome observed during HF STN DBS in PD patients. Therefore, the classical rate model does not convincingly explain the therapeutic effects of HF STN DBS and these observations suggested that it is not just the firing rate, but also the pattern of neural firing that needs to be considered to explain the therapeutic mechanism of HF STN DBS.

Rubin and Terman (RT) (Rubin & Terman, 2004) developed a biophysical computational model of the BG network. In the PD state, the BG neurons exhibit more burst-like firing, and this pattern of activity was included in the RT model. However, despite representation of the activity patterns observed during PD, the RT model did not reproduce the frequency dependent effects of STN DBS on PD symptoms (So, Kent, et al., 2012), as frequencies as low as 20 Hz were effective in suppressing a model proxy for symptom, which is inconsistent with clinical observations (Birdno & Grill, 2008). So et al. (So, Kent, et al., 2012) revised the properties of the RT model to account for the frequency-dependent effects of STN DBS. However, the firing rates and patterns of activity observed in model BG neurons during PD in the revised model are not consistent with those seen in the 6-OHDA lesioned rat.

Kang and Lowery developed a biophysical model of the cortico-BG-thalamic circuit that included the hyperdirect pathway (Kang & Lowery, 2013). Although the model accounted for pathological oscillatory activity similar to that seen in PD, the model was not validated against experimental data, and the firing rate of GPi neurons in the model was comparable to those seen in non-human primates rather than rats. The cortico-basal ganglia-thalamic model that we developed was validated both at the cellular and network levels and reproduced key features of experimental data from the 6-OHDA lesioned rat model of PD.

#### 5.4 Mechanism of STN DBS

At least three sites are possible sources of pathological low-frequency oscillatory activity in PD. Firstly, cortical neurons exhibit synchronous beta oscillations in PD, as seen in CTX local field potentials in 6-OHDA lesioned rats (Mallet, Pogosyan, Sharott, et al., 2008), and there is evidence for generation of the beta rhythm in CTX (Yamawaki et al., 2008). Hence, the CTX is a

1  
2  
3  
4 potential source of low-frequency oscillations in the PD state independent of its synaptic inputs.  
5  
6 A second possible source of pathological low-frequency oscillations is the Str (McCarthy et al.,  
7  
8 2011), as an increase in Str ACh as a result of dopamine loss is sufficient for Str neurons to  
9  
10 generate oscillations in the 8-30Hz band. Finally, the reciprocally connected STN-GPe network is  
11  
12 capable of generating oscillations without any synaptic inputs from the CTX or Str (Plenz & Kital,  
13  
14 1999). In the model, BG beta band oscillatory activity was suppressed when the NMDA synaptic  
15  
16 conductance of the hyperdirect pathway was reduced. Hence, the model supports the  
17  
18 hypothesis that beta oscillatory activity generated in the CTX enters the BG through the STN,  
19  
20 which receive strong excitatory projections from the CTX, and oscillatory input from STN drives  
21  
22 GPe and GPi to oscillate in the beta band as observed in the 6-OHDA lesioned rat (Moran et al.,  
23  
24 2011).

31  
32  
33 Regardless of the source, propagation of pathological low-frequency oscillatory activity  
34  
35 to the GPi occurs through the STN, and this might explain why surgical interventions involving  
36  
37 the STN are effective for relieving PD motor symptoms. STN lesion silences its efferents to GPi  
38  
39 and GPe, such that pathological low-frequency oscillatory activity cannot reach the output of  
40  
41 the BG. In the model, HF STN DBS suppressed pathological low-frequency oscillations by  
42  
43 exciting some GPi neurons through the STN-GPi pathway and inhibiting other GPi neurons  
44  
45 through the STN-GPe-GPi pathway. Excited GPi neurons showed a decrease in pathological  
46  
47 burst activity and exhibited a more regularized firing, while inhibited GPi neurons simply did not  
48  
49 transmit the pathological activity to the TH. A greater proportion of neurons were inhibited and  
50  
51 excited during effective HF STN DBS when compared to ineffective LF STN DBS. Therefore, the  
52  
53 therapeutic effects of HF STN DBS might arise from the ability to both excite and inhibit greater  
54  
55  
56  
57  
58  
59  
60  
61

numbers of neurons in the output nucleus of the BG through the STN-GPe and STN-GPe-GPi pathway when compared to LF STN DBS. The STN is strategically located and able to influence GPI neurons both directly and indirectly. Behaviorally effective HF STN DBS in 6-OHDA-lesioned rats resulted in both excitation and inhibition of SNr neurons similar to those observed in the model (Bosch et al., 2011). The excitation and inhibition of SNr neurons during STN DBS was due to the activation of STN efferents to SNr and GPe efferents to SNr passing through STN respectively. The same study also showed an increase in the number of SNr neurons being inhibited and excited during HF STN DBS than during LF STN DBS.

1  
2  
3  
4  
5  
6  
7 **Fig. 1** Cortical-basal ganglia-thalamus network model. (A) Model schematic showing  
8 connections within the network. (B) Details of synaptic connections within the network model.  
9 Each rCortex neuron receives excitatory input from one TH neuron and inhibitory input from  
10 four randomly selected iCortex neurons. Each iCortex neuron receives excitatory input from  
11 four randomly selected rCortex neurons. Each dStr neuron receives excitatory input from one  
12 rCortex neuron and inhibitory axonal collaterals from three randomly selected dStr neurons.  
13 Each idStr neuron receives excitatory input from one rCortex neuron and inhibitory axonal  
14 collaterals from four randomly selected idStr neurons. Each STN neuron receives inhibitory  
15 input from two GPe neurons and excitatory input from two rCortex neurons. Each GPe neuron  
16 receives inhibitory axonal collaterals from any two other GPe neurons and inhibitory input from  
17 all idStr neurons. Each GPi neuron receives inhibitory input from two GPe neurons and  
18 inhibitory input from all dStr neurons. Some GPe/GPi neurons receive excitatory input from two  
19 STN neurons, while others do not. Each TH neuron receives inhibitory input from one GPi  
20 neuron  
21  
22  
23  
24  
25  
26

27 **Fig. 2** Str responses to CTX stimulation. (A) Model Str PSTH obtained under normal conditions  
28 shows strong excitation following CTX stimulation. Str neurons are not spontaneously active  
29 under normal conditions. (B) Model Str PSTH obtained during PD state shows strong excitation  
30 and long inhibition following CTX stimulation. Str neurons exhibit increased spontaneous firing  
31 during PD. (C,D) Experimental PSTHs (Kita & Kita, 2011) match well with model results  
32  
33

34 **Fig. 3** STN responses to CTX stimulation. (A) Model STN PSTH obtained under normal conditions  
35 shows early excitation and late excitation following CTX stimulation. (B) Model STN PSTH  
36 obtained during PD state shows early excitation, late excitation and long inhibition following  
37 CTX stimulation. (C,D) Model PSTHs are comparable with PSTHs obtained from an experimental  
38 study (Kita & Kita, 2011)  
39  
40

41 **Fig. 4** GPe responses to CTX stimulation. (A) Model GPe PSTH obtained under normal condition  
42 shows early excitation, short inhibition and weak late excitation following CTX stimulation. (B)  
43 Model GPe PSTH obtained during PD state shows weak early excitation, short inhibition and  
44 strong late excitation following CTX stimulation. (C,D) Model PSTHs are comparable with PSTHs  
45 obtained from an experimental study (Kita & Kita, 2011)  
46  
47

48 **Fig. 5** GPi responses to CTX stimulation. (A,C) Model GPi PSTHs obtained under normal  
49 conditions show either early excitation, short inhibition and late excitation or short inhibition  
50 and late excitation following CTX stimulation. (B,D) Model GPi PSTHs obtained during PD state  
51 show either early excitation and long inhibition or only long inhibition following CTX  
52 stimulation. (E,F,G,H) Model PSTHs are comparable with PSTHs obtained from an experimental  
53 study (Kita & Kita, 2011)  
54  
55  
56  
57  
58  
59  
60  
61  
62  
63  
64  
65

1  
2  
3  
4 **Fig. 6** Firing rates of model and experimental (Kita & Kita, 2011) neurons in striatum (Str),  
5 subthalamic nucleus (STN), globus pallidus externa (GPe) and globus pallidus interna (GPi)  
6 under normal and PD conditions. Standard error bars for model data are shown for 10 ten-  
7 second simulations under each condition  
8  
9

10  
11 **Fig. 7** Firing patterns of STN, GPe and GPi neurons. Single units and rastergrams under normal,  
12 PD, and PD condition with 130 Hz STN DBS. During the PD state, neurons fired in a more  
13 rhythmic burst fashion, while 130 Hz STN DBS suppressed these bursts by either exciting or  
14 inhibiting the firing of GPe/GPi neurons  
15  
16

17 **Fig. 8** Oscillatory activity across BG nuclei during normal, PD and 130 Hz STN DBS. (A,B,C) Power  
18 spectra (PS) of STN, GPe and GPi spike times show exaggerated oscillatory activity in both the  
19 alpha and beta band during PD conditions when compared to the normal state. PSs show the  
20 suppression of these pathological alpha and beta oscillations during HF STN DBS across all BG  
21 nuclei  
22  
23

24 **Fig. 9** Alpha and beta band oscillatory activity during PD condition in model BG neurons. (A,B)  
25 Spectrograms of STN, GPi spike times exhibit prominent oscillations in both the alpha and beta  
26 band. Oscillatory activity in the beta band at 20Hz is interrupted by periods of low-frequency  
27 oscillation at 9Hz. (C) Spectrogram of STN spike times shows suppression of STN beta band  
28 oscillations following reduction of NMDA-R synaptic conductance in STN to zero (mimicking  
29 NMDA antagonist infusion) at 1sec. NMDA antagonist did not have any effect on the STN  
30 oscillatory activity at 9Hz  
31  
32

33 **Fig. 10** Effects of STN DBS frequency on pallidal neurons firing rate. (A,B) Mean firing rate of  
34 model GPe/GPi neurons. There was no significant difference in the mean firing rates of the  
35 model GPe/GPi neurons at all STN DBS frequencies. Standard error bars are shown for 10 ten-  
36 second simulations for each stimulus frequency. (C,D) Firing rate of individual GPe/GPi neurons  
37 normalized by the firing rate of the neuron during PD. Colormap is sorted from most inhibitory  
38 to most excitatory response at each stimulus frequency. Note the activity of a greater number  
39 of GPe/GPi neurons being influenced during HF STN DBS then during LF STN DBS  
40  
41

42 **Fig. 11** Effect of STN DBS frequency on GPi low-frequency oscillatory activity. (A,B,C,D)  
43 Spectrograms of GPi spike times during PD and three different STN DBS stimulus frequencies  
44 (10 Hz, 45 Hz and 130 Hz). During PD, GPi neurons exhibited synchronized oscillatory activity in  
45 both the alpha and beta band. 10 Hz STN DBS slightly increased this oscillatory activity.  
46 Although 45 Hz STN DBS reduced the GPi oscillatory activity, it did not completely suppress the  
47 oscillations. 130 Hz STN DBS completely suppressed the GPi oscillations and reversed PD  
48 symptoms. (E) Effect of STN DBS frequency on model GPi neurons 7-35Hz power. Standard  
49 error bars are shown for 10 ten-second simulations for each stimulus frequency  
50  
51

1  
2  
3  
4 **Fig. 12** Frequency-dependent effects of STN DBS on GPi responses evoked by CTX stimulation.  
5 (A) PSTHs showing CTX stimulation evoked GPi activity at various STN DBS frequencies. (B)  
6 PSTHs showing CTX stimulation induced GPi responses under normal, PD and 130 Hz STN DBS  
7 conditions. 130 Hz STN DBS effectively normalized the enhanced late inhibition observed in GPi  
8 response relative to PD. However, 130 Hz STN DBS failed to restore the early short inhibition  
9 seen in the GPi response under normal conditions. Arrow indicates the time (100 ms) at which  
10 the CTX was stimulated by a single pulse. (C,D) 130 Hz STN DBS reduced both the strength and  
11 duration of late inhibition which were exaggerated during PD to values similar to those seen  
12 under normal conditions  
13  
14  
15  
16  
17  
18  
19  
20  
21  
22  
23  
24  
25  
26  
27  
28  
29  
30  
31  
32  
33  
34  
35  
36  
37  
38  
39  
40  
41  
42  
43  
44  
45  
46  
47  
48  
49  
50  
51  
52  
53  
54  
55  
56  
57  
58  
59  
60  
61  
62  
63  
64  
65

## References

- Agid, Y., Javoy-Agid, F., & Ruberg, M. (1987). Biochemistry of neurotransmitters in Parkinson's disease. *Movement disorders*, 2(7), 166-230.
- Albin, R. L., Young, A. B., & Penney, J. B. (1989). The functional anatomy of basal ganglia disorders. *Trends in neurosciences*, 12(10), 366-375.
- Anderson, M. E., Postupna, N., & Ruffo, M. (2003). Effects of high-frequency stimulation in the internal globus pallidus on the activity of thalamic neurons in the awake monkey. *Journal of neurophysiology*, 89(2), 1150-1160.
- Baufreton, J., Kirkham, E., Atherton, J. F., Menard, A., Magill, P. J., Bolam, J. P., & Bevan, M. D. (2009). Sparse but selective and potent synaptic transmission from the globus pallidus to the subthalamic nucleus. *Journal of neurophysiology*, 102(1), 532-545.
- Bergman, H., Wichmann, T., Karmon, B., & DeLong, M. (1994). The primate subthalamic nucleus. II. Neuronal activity in the MPTP model of parkinsonism. *Journal of neurophysiology*, 72(2), 507-520.
- Birdno, M. J., & Grill, W. M. (2008). Mechanisms of deep brain stimulation in movement disorders as revealed by changes in stimulus frequency. *Neurotherapeutics*, 5(1), 14-25.
- Blesa, J., & Przedborski, S. (2014). Parkinson's disease: animal models and dopaminergic cell vulnerability. *Frontiers in neuroanatomy*, 8.
- Bolam, J., Hanley, J., Booth, P., & Bevan, M. (2000). Synaptic organisation of the basal ganglia. *Journal of anatomy*, 196(04), 527-542.
- Bosch, C., Degos, B., Deniau, J.-M., & Venance, L. (2011). Subthalamic nucleus high-frequency stimulation generates a concomitant synaptic excitation-inhibition in substantia nigra pars reticulata. *The Journal of physiology*, 589(17), 4189-4207.
- Brocker, D. T., Swan, B. D., Turner, D. A., Gross, R. E., Tatter, S. B., Miller Koop, M., . . . Grill, W. M. (2013). Improved efficacy of temporally non-regular deep brain stimulation in Parkinson's disease. *Experimental neurology*, 239, 60-67.
- Brown, D. A. (2010). Muscarinic acetylcholine receptors (mAChRs) in the nervous system: some functions and mechanisms. *Journal of molecular neuroscience*, 41(3), 340-346.
- Chang, H., & Kitai, S. (1985). Projection neurons of the nucleus accumbens: an intracellular labeling study. *Brain research*, 347(1), 112-116.
- Chang, H., Wilson, C., & Kitai, S. (1982). A Golgi study of rat neostriatal neurons: light microscopic analysis. *Journal of Comparative Neurology*, 208(2), 107-126.
- Cruz, A. V., Mallet, N., Magill, P. J., Brown, P., & Averbeck, B. B. (2012). Effects of dopamine depletion on information flow. *PNAS*, 109(44), 18126-18131.
- Degos, B., Deniau, J.-M., Thierry, A.-M., Glowinski, J., Pezard, L., & Maurice, N. (2005). Neuroleptic-induced catalepsy: electrophysiological mechanisms of functional recovery induced by high-frequency stimulation of the subthalamic nucleus. *The Journal of neuroscience*, 25(33), 7687-7696.
- DeLong, M. R. (1990). Primate models of movement disorders of basal ganglia origin. *Trends in neurosciences*, 13(7), 281-285.

- Dorval, A. D., Russo, G. S., Hashimoto, T., Xu, W., Grill, W. M., & Vitek, J. L. (2008). Deep brain stimulation reduces neuronal entropy in the MPTP-primate model of Parkinson's disease. *Journal of neurophysiology*, 100(5), 2807-2818.
- Farries, M. A., Kita, H., & Wilson, C. J. (2010). Dynamic spike threshold and zero membrane slope conductance shape the response of subthalamic neurons to cortical input. *The Journal of neuroscience*, 30(39), 13180-13191.
- Fogelson, N., Kühn, A. A., Silberstein, P., Limousin, P. D., Hariz, M., Trottenberg, T., . . . Brown, P. (2005). Frequency dependent effects of subthalamic nucleus stimulation in Parkinson's disease. *Neuroscience letters*, 382(1), 5-9.
- Fujimoto, K., & Kita, H. (1993). Response characteristics of subthalamic neurons to the stimulation of the sensorimotor cortex in the rat. *Brain research*, 609(1), 185-192.
- Götz, T., Kraushaar, U., Geiger, J., Lübke, J., Berger, T., & Jonas, P. (1997). Functional properties of AMPA and NMDA receptors expressed in identified types of basal ganglia neurons. *The Journal of neuroscience*, 17(1), 204-215.
- Grill, W. M., Snyder, A. N., & Miocinovic, S. (2004). Deep brain stimulation creates an informational lesion of the stimulated nucleus. *Neuroreport*, 15(7), 1137-1140.
- Hammond, C., Bergman, H., & Brown, P. (2007). Pathological synchronization in Parkinson's disease: networks, models and treatments. *Trends in neurosciences*, 30(7), 357-364.
- Hashimoto, T., Elder, C. M., Okun, M. S., Patrick, S. K., & Vitek, J. L. (2003). Stimulation of the subthalamic nucleus changes the firing pattern of pallidal neurons. *The Journal of neuroscience*, 23(5), 1916-1923.
- Hollerman, J. R., & Grace, A. A. (1992). Subthalamic nucleus cell firing in the 6-OHDA-treated rat: basal activity and response to haloperidol. *Brain research*, 590(1), 291-299.
- Hornykiewicz, O. (1998). Biochemical aspects of Parkinson's disease. *Neurology*, 51(2 Suppl 2), S2-S9.
- Ikarashi, Y., Takahashi, A., Ishimaru, H., Arai, T., & Maruyama, Y. (1997). Regulation of Dopamine D<sub>1</sub> and D<sub>2</sub> Receptors on Striatal Acetylcholine Release in Rats. *Brain research bulletin*, 43(1), 107-115.
- Izhikevich, E. M. (2003). Simple model of spiking neurons. *IEEE Transactions on neural networks*, 14(6), 1569-1572.
- Jankovic, J., Rajput, A. H., McDermott, M. P., & Perl, D. P. (2000). The evolution of diagnosis in early Parkinson disease. *Archives of neurology*, 57(3), 369-372.
- Kang, G., & Lowery, M. M. (2013). Interaction of oscillations, and their suppression via deep brain stimulation, in a model of the cortico-basal ganglia network. *Neural Systems and Rehabilitation Engineering, IEEE Transactions on*, 21(2), 244-253.
- Kita, H. (2001). Neostriatal and globus pallidus stimulation induced inhibitory postsynaptic potentials in entopeduncular neurons in rat brain slice preparations. *Neuroscience*, 105(4), 871-879.
- Kita, H., & Kita, T. (2011). Cortical stimulation evokes abnormal responses in the dopamine-depleted rat basal ganglia. *The Journal of neuroscience*, 31(28), 10311-10322.

- 1  
2  
3  
4 Kita, H., & Kitai, S. (1991). Intracellular study of rat globus pallidus neurons: membrane  
5 properties and responses to neostriatal, subthalamic and nigral stimulation. *Brain research*,  
6 564(2), 296-305.  
7  
8 Kühn, A. A., Kempf, F., Brücke, C., Doyle, L. G., Martinez-Torres, I., Pogosyan, A., . . . Hariz, M.  
9 I. (2008). High-frequency stimulation of the subthalamic nucleus suppresses oscillatory  $\beta$   
10 activity in patients with Parkinson's disease in parallel with improvement in motor  
11 performance. *The Journal of neuroscience*, 28(24), 6165-6173.  
12  
13 Levy, R., Ashby, P., Hutchison, W. D., Lang, A. E., Lozano, A. M., & Dostrovsky, J. O. (2002).  
14 Dependence of subthalamic nucleus oscillations on movement and dopamine in Parkinson's  
15 disease. *Brain*, 125(6), 1196-1209.  
16  
17 Li, Q., Ke, Y., Chan, D. C., Qian, Z.-M., Yung, K. K., Ko, H., . . . Yung, W.-H. (2012). Therapeutic  
18 deep brain stimulation in Parkinsonian rats directly influences motor cortex. *Neuron*, 76(5),  
19 1030-1041.  
20  
21 Mallet, N., Ballion, B., Le Moine, C., & Gonon, F. (2006). Cortical inputs and GABA  
22 interneurons imbalance projection neurons in the striatum of parkinsonian rats. *The Journal of*  
23 *neuroscience*, 26(14), 3875-3884.  
24  
25 Mallet, N., Pogosyan, A., Márton, L. F., Bolam, J. P., Brown, P., & Magill, P. J. (2008).  
26 Parkinsonian beta oscillations in the external globus pallidus and their relationship with  
27 subthalamic nucleus activity. *The Journal of neuroscience*, 28(52), 14245-14258.  
28  
29 Mallet, N., Pogosyan, A., Sharott, A., Csicsvari, J., Bolam, J. P., Brown, P., & Magill, P. J. (2008).  
30 Disrupted dopamine transmission and the emergence of exaggerated beta oscillations in  
31 subthalamic nucleus and cerebral cortex. *The Journal of neuroscience*, 28(18), 4795-4806.  
32  
33 Marsden, C., Parkes, J., & Quinn, N. (1982). Fluctuations of disability in Parkinson's disease:  
34 clinical aspects. *Movement disorders*. London: Butterworth, 198(1), 96-122.  
35  
36 McCarthy, M., Moore-Kochlacs, C., Gu, X., Boyden, E., Han, X., & Kopell, N. (2011). Striatal  
37 origin of the pathologic beta oscillations in Parkinson's disease. *Proceedings of the National*  
38 *Academy of Sciences*, 108(28), 11620-11625.  
39  
40 McConnell, G. C., So, R. Q., Hilliard, J. D., Lopomo, P., & Grill, W. M. (2012). Effective deep  
41 brain stimulation suppresses low-frequency network oscillations in the basal ganglia by  
42 regularizing neural firing patterns. *The Journal of neuroscience*, 32(45), 15657-15668.  
43  
44 Miguelez, C., Morin, S., Martinez, A., Goillandeau, M., Bezard, E., Bioulac, B., & Baufreton, J.  
45 (2012). Altered pallido-pallidal synaptic transmission leads to aberrant firing of globus pallidus  
46 neurons in a rat model of Parkinson's disease. *The Journal of physiology*, 590(22), 5861-5875.  
47  
48 Moran, R. J., Mallet, N., Litvak, V., Dolan, R. J., Magill, P. J., Friston, K. J., & Brown, P. (2011).  
49 Alterations in brain connectivity underlying beta oscillations in Parkinsonism. *PLoS*  
50 *computational biology*, 7(8), e1002124.  
51  
52 Moro, E., Lozano, A. M., Pollak, P., Agid, Y., Rehncrona, S., Volkmann, J., . . . Hariz, M. I. (2010).  
53 Long-term results of a multicenter study on subthalamic and pallidal stimulation in Parkinson's  
54 disease. *Movement disorders*, 25(5), 578-586.  
55  
56 Nakanishi, H., Kita, H., & Kitai, S. (1987). Intracellular study of rat substantia nigra pars  
57 reticulata neurons in an in vitro slice preparation: electrical membrane properties and response  
58 characteristics to subthalamic stimulation. *Brain research*, 437(1), 45-55.

- Nakanishi, H., Kita, H., & Kitai, S. (1991). Intracellular study of rat entopeduncular nucleus neurons in an in vitro slice preparation: response to subthalamic stimulation. *Brain research*, 549(2), 285-291.
- Nambu, A., Tokuno, H., Hamada, I., Kita, H., Imanishi, M., Akazawa, T., . . . Hasegawa, N. (2000). Excitatory cortical inputs to pallidal neurons via the subthalamic nucleus in the monkey. *Journal of neurophysiology*, 84(1), 289-300.
- Nambu, A., Tokuno, H., & Takada, M. (2002). Functional significance of the cortico-subthalamo-pallidal 'hyperdirect' pathway. *Neuroscience research*, 43(2), 111-117.
- Nicola, S. M., Surmeier, D. J., & Malenka, R. C. (2000). Dopaminergic modulation of neuronal excitability in the striatum and nucleus accumbens. *Annual review of neuroscience*, 23(1), 185-215.
- Otsuka, T., Abe, T., Tsukagawa, T., & Song, W.-J. (2004). Conductance-based model of the voltage-dependent generation of a plateau potential in subthalamic neurons. *Journal of neurophysiology*, 92(1), 255-264.
- Pan, M.-K., Tai, C.-H., Liu, W.-C., Pei, J.-C., Lai, W.-S., & Kuo, C.-C. (2014). Deranged NMDAergic cortico-subthalamic transmission underlies parkinsonian motor deficits. *The Journal of clinical investigation*, 124(10), 4629.
- Pang, Z., Ling, G. Y., Gajendiran, M., & Xu, Z. C. (2001). Enhanced excitatory synaptic transmission in spiny neurons of rat striatum after unilateral dopamine denervation. *Neuroscience letters*, 308(3), 201-205.
- Plenz, D., & Kitai, S. T. (1999). A basal ganglia pacemaker formed by the subthalamic nucleus and external globus pallidus. *Nature*, 400(6745), 677-682.
- Quinn, N., Luthert, P., Honavar, M., & Marsden, C. (1989). Pure akinesia due to Lewy body Parkinson's disease: a case with pathology. *Movement disorders*, 4(1), 85-89.
- Rajput, A., Sitte, H., Rajput, A., Fenton, M., Piñel, C., & Hornykiewicz, O. (2008). Globus pallidus dopamine and Parkinson motor subtypes Clinical and brain biochemical correlation. *Neurology*, 70(16 Part 2), 1403-1410.
- Raz, A., Vaadia, E., & Bergman, H. (2000). Firing patterns and correlations of spontaneous discharge of pallidal neurons in the normal and the tremulous 1-methyl-4-phenyl-1, 2, 3, 6-tetrahydropyridine vervet model of parkinsonism. *The Journal of neuroscience*, 20(22), 8559-8571.
- Rubin, J. E., & Terman, D. (2004). High frequency stimulation of the subthalamic nucleus eliminates pathological thalamic rhythmicity in a computational model. *Journal of computational neuroscience*, 16(3), 211-235.
- Ryan, L., & Clark, K. (1991). The role of the subthalamic nucleus in the response of globus pallidus neurons to stimulation of the prelimbic and agranular frontal cortices in rats. *Experimental brain research*, 86(3), 641-651.
- Ryu, S. B., Bae, E. K., Kim, J., Hwang, Y. S., Im, C., Chang, J. W., . . . Kim, K. H. (2013). Neuronal Responses in the Globus Pallidus during Subthalamic Nucleus Electrical Stimulation in Normal and Parkinson's Disease Model Rats. *The Korean Journal of Physiology & Pharmacology*, 17(4), 299-306.
- Shaw, F.-Z., & Liao, Y.-F. (2005). Relation between activities of the cortex and vibrissae muscles during high-voltage rhythmic spike discharges in rats. *Journal of neurophysiology*, 93(5), 2435-2448.

- 1  
2  
3  
4 Sims, R. E., Woodhall, G. L., Wilson, C. L., & Stanford, I. M. (2008). Functional characterization  
5 of GABAergic pallidopallidal and striatopallidal synapses in the rat globus pallidus *in vitro*.  
6 *European journal of neuroscience*, 28(12), 2401-2408.  
7  
8 So, R. Q., Kent, A. R., & Grill, W. M. (2012). Relative contributions of local cell and passing fiber  
9 activation and silencing to changes in thalamic fidelity during deep brain stimulation and  
10 lesioning: a computational modeling study. *Journal of computational neuroscience*, 32(3), 499-519.  
11  
12 So, R. Q., McConnell, G. C., August, A. T., & Grill, W. M. (2012). Characterizing effects of  
13 subthalamic nucleus deep brain stimulation on methamphetamine-induced circling behavior in  
14 hemi-Parkinsonian rats. *Neural Systems and Rehabilitation Engineering, IEEE Transactions on*, 20(5),  
15 626-635.  
16  
17 Taverna, S., Ilijic, E., & Surmeier, D. J. (2008). Recurrent collateral connections of striatal  
18 medium spiny neurons are disrupted in models of Parkinson's disease. *The Journal of*  
19 *neuroscience*, 28(21), 5504-5512.  
20  
21 Timmermann, L., Wojtecki, L., Gross, J., Lehrke, R., Voges, J., Maarouf, M., . . . Schnitzler, A.  
22 (2004). Ten-Hertz stimulation of subthalamic nucleus deteriorates motor symptoms in  
23 Parkinson's disease. *Movement disorders*, 19(11), 1328-1333.  
24  
25 Tremblay, L., & Filion, M. (1989). Responses of pallidal neurons to striatal stimulation in  
26 monkeys with MPTP-induced parkinsonism. *Brain research*, 498(1), 17-33.  
27  
28 Walker, H. C., Huang, H., Gonzalez, C. L., Bryant, J. E., Killen, J., Knowlton, R. C., . . . Guthrie,  
29 B. L. (2012). Short latency activation of cortex by clinically effective thalamic brain stimulation  
30 for tremor. *Movement disorders*, 27(11), 1404-1412.  
31  
32 Weaver, F. M., Follett, K., Stern, M., Hur, K., Harris, C., Marks, W. J., . . . Moy, C. S. (2009).  
33 Bilateral deep brain stimulation vs best medical therapy for patients with advanced Parkinson  
34 disease: a randomized controlled trial. *Jama*, 301(1), 63-73.  
35  
36 Wichmann, T., & Soares, J. (2006). Neuronal firing before and after burst discharges in the  
37 monkey basal ganglia is predictably patterned in the normal state and altered in parkinsonism.  
38 *Journal of neurophysiology*, 95(4), 2120-2133.  
39  
40 Xu, W., Russo, G. S., Hashimoto, T., Zhang, J., & Vitek, J. L. (2008). Subthalamic nucleus  
41 stimulation modulates thalamic neuronal activity. *The Journal of neuroscience*, 28(46), 11916-  
42 11924.  
43  
44 Yamawaki, N., Stanford, I. M., Hall, S. D., & Woodhall, G. L. (2008). Pharmacologically induced  
45 and stimulus evoked rhythmic neuronal oscillatory activity in the primary motor cortex<i>*i*</i>  
46 *in vitro*</i>. *Neuroscience*, 151(2), 386-395.  
47  
48  
49  
50  
51  
52  
53  
54  
55  
56  
57  
58  
59  
60  
61  
62  
63  
64  
65



Click here to access/download  
**Supplemental Materials (Optional)**  
Appendix\_A.docx